Construction and Building Materials 344 (2022) 128032

Contents lists available at ScienceDirect

Construction and Building Materials

journal homepage: www.elsevier.com/locate/conbuildmat

Experimental and numerical modal analysis of a cross laminated timber floor system in different construction states

Michael Kawrza, Thomas Furtmüller, Christoph Adam *

Unit of Applied Mechanics, University of Innsbruck, Technikerstr. 13, 6020 Innsbruck, Austria

ARTICLE INFO

Keywords:
Cross laminated timber slab
Floor construction
Footfall sound insulation
Modal analysis
Optimization

ABSTRACT

This paper addresses the vibration characteristics of a cross laminated timber (CLT) floor in a residential building during three construction states. Experimental modal analyses are carried out on the blank CLT slab, on the slab with added drywall ceiling, and on the slab with drywall ceiling and added floating screed. A reliable numerical model of the system is created with the means of a finite element model updating procedure. This model shows that some experimentally determined modes can be attributed to the dynamic interaction with the shaker used for excitation during the tests. In the finite element model, this effect can subsequently be eliminated. Based on the validated numerical model, the impact of various parameters of the floor construction on the low-frequency footfall sound insulation is investigated.

1. Introduction

In recent decades, timber construction has developed into a competitive alternative to traditional masonry and reinforced concrete construction in both industrial and residential housing. Especially since the introduction of cross laminated timber (CLT), a solid wood panel usually consisting of 3, 5 or 7 layers of lamellas glued together on their side faces and stacked perpendicular to each other [1,2], the application range of timber construction is expanding from single to multi-story buildings, as shown for example by an 18-story multi-purpose timber building in Norway [3] or an 18-story student dormitory at the University of British Columbia in Vancouver [4]. However, compared to reinforced concrete, these lightweight structures have a high stiffness-to-weight ratio, which makes these structures more prone to vibrations. For the construction of larger and taller buildings, it is therefore necessary to understand the dynamic behavior of timber structural systems in order to avoid damage to structural and non-structural components [5]. In addition to lateral deflection, transversal vibrations must also be taken into account in the design of these structures. Particularly in urban living settings with a large number of dwellings in multi-story buildings, occupants potentially face two major problems with timber floor systems: Floor vibrations and structure-borne noise.

In residential buildings, vibrations are mainly induced by walking, running or jumping persons and falling objects. Especially at low frequencies, vibrations can cause severe discomfort to occupants when natural frequencies in the human body are stimulated [6]. The vibrations propagate through the floor system and excite the air in adjacent rooms, resulting in potentially disturbing footfall sound [7]. To minimize the impact of floor vibrations on occupants, applicable standards, e.g. Eurocode 5 [8], suggest a lower limit of 8 Hz for the fundamental frequency of timber floor systems with an additional stiffness criterion to limit deflection and the maximum velocity resulting from an impulse of 1 Ns. In addition, standardized methods for predicting the fundamental frequency of rectangular simply supported slabs are outlined. However, these methods are strongly influenced by the assumed material properties, which vary greatly due to density properties, moisture content and inhomogeneities [9]) and neglect the flexibility of the supports. Due to this variation [10], there are a number of destructive and non-destructive methods for determining the elastic properties of wood-based materials. Examples of non destructive methods to identify material properties of structural timber beams can be found in [11], where the modal properties of the test specimens are determined using experimental modal analysis and the elastic properties are identified as part of a model updating process, and in [12], where elastic properties of CLT panels are obtained.

As a result of this uncertainty in material parameters and the need to accurately predict the dynamic response of timber floors, numerous systems have been studied experimentally under laboratory and in-situ conditions to gain insight into the dynamic properties. In [13,14] experimental and numerical investigations were carried out on a number of timber floors with different floor construction and boundary conditions in order to develop guidelines for the design of timber floors to avoid disturbing vibrations. [15,16] tested CLT floors

* Corresponding author.
E-mail address: christoph.adam@uibk.ac.at (C. Adam).

https://doi.org/10.1016/j.conbuildmat.2022.128032
Received 21 September 2021; Received in revised form 26 May 2022; Accepted 31 May 2022

with different boundary conditions, CLT types and plan aspect ratios under laboratory conditions, in [17] dynamic properties of a timber floor system were investigated under laboratory and in-situ conditions during the construction phase, in [18] a detailed experimental modal analysis and model updating is presented on a point-supported slab without joists consisting of seven CLT panels, and in [19] floor vibrations of a glued-laminated-timber beam and deck floor are evaluated. Also under laboratory conditions, in [20] timber floor modules were investigated experimentally and analytically, comparing five analytical prediction methods for the natural frequencies with the experimentally determined natural frequencies. A common result of all these studies is that the boundary conditions have a significant impact on the modal properties of the investigated floors. In order to adequately predict the dynamic response numerically, the boundary conditions must be carefully considered in the model.

To overcome the issue of structure-borne noise, structural elements must comply with limits for impact sound insulation, which are assessed using a standardized single value rating [21] of measurements with a standardized impact tapping machine or rubber ball [22]. The sound insulation requirements are based on the vibration performance of traditional concrete structures and therefore evaluated in a frequency range of 100–3150 Hz. Applying the same methods to lightweight structures leads to inadequate impact sound insulation, even in the extended frequency range of 50–3150 Hz, due to the poor vibro-acoustic performance of timber floors in a frequency range below 125 Hz, compared to concrete heavy weight floors. Therefore, studies evaluating the impact sound insulation of timber floors subjectively and objectively [23–25] suggest the consideration of frequencies down to 20 Hz.

In this contribution, the dynamic behavior of a CLT floor system with different boundary conditions in different construction states is investigated. For each construction state, a detailed experimental modal analysis (EMA) is performed to determine the natural frequencies in the low-frequency range with corresponding damping ratios and mode shapes. In addition, the collected data form the basis for a model updating procedure to calibrate finite element (FE) models. The objectives of this study are (*i*) to gain insight into the dynamic behavior of a CLT floor system at different construction states and to experimentally identify the influence of the boundary conditions, (*ii*) to identify a robust and representative parameter set for FE models, which numerically accurately predicts the experimental outcome, and (*iii*) to investigate the influence of structural and non-structural components such as the material properties of the CLT, the elastic fill or the screed thickness with the updated FE models. The ultimate goal is to assess more realistically the low-frequency performance of the CLT floor system.

The paper is structured as follows. In Section 2 the test object is outlined. The experimental and numerical methods used with the theoretical basis are explained in Section 3. Section 4 describes the results of the EMA, while Section 5 addresses the model updating of the FE model of the test object in the considered construction states. Based on the optimized FE model for the completed floor system in the third construction state, in Section 6 selected parameter studies are conducted to reveal the influence of material properties and different compositions of the floor construction on the vibration performance in the low-frequency range.

2. Test object

In the course of the reconstruction and renovation of an old farm house in the province of Tyrol, Austria, the barn shown in Fig. 1 was converted so that it could accommodate three apartments. To separate the apartment on the first floor from the one on the second floor, a floor system of CLT was installed.

During the construction phase, dynamic measurements were carried out on this slab in three different construction states. These three

Fig. 1. Original farm building before renovation (copyright M. Flach).

construction states are referred to in the following as state 1, state 2 and state 3.

In state 1, shown in the left photo of Fig. 2, only the raw CLT slab was installed without drywall ceiling, partition wall and floating screed. The floor plan of the CLT slab approximates a rectangle with roughly 7 by 8 m dimensions, with lower edge slightly skewed, outer edge at about 45° on the lower left corner and a rectangular recess on the right edge, as can be seen in Fig. 3. This figure also shows that the slab consists of three panels. Each of the panels is made of 5-ply CLT of strength class C24 [26] with a layer thickness of 0.04 m, resulting in a total thickness of 0.2 m. The three panels are connected to each other by eight-millimeter fully threaded screws with a length of 240 millimeters, arranged in pairs at a distance of 0.2 m, inclined at 45° and perpendicular to each other, see also Fig. 3. Since the floor was installed in an existing building, the boundary conditions are inhomogeneous. It should be emphasized, however, that the authors of this contribution had no influence on the design of the various supports and therefore take them as given. Near its center, the slab is point-supported on a wooden column with a diameter of 0.2 m, reinforced by a star-shaped steel connector [27,28] on the surface of the slab. At the outer edges, the slab is supported on a solid timber wall (upper edge in Fig. 3), on a glued laminated joist (upper part of the left edge in Fig. 3) or on L-shaped steel profiles attached to load bearing walls. A sound-absorbing polyurethane compound with a thickness of six millimeters is sandwiched between the support surface of the CLT and the supporting structure.

In state 2, the CLT slab is equipped with a drywall ceiling of gypsum fiber boards and a non-structural lightweight timber wall rests on top of the slab, whose position is shown in 3. The gypsum fiber boards are stapled to spruce battens with a cross-section of 0.03 m × 0.06 m, which are attached to the bottom of the CLT panel. The partition wall consists of structural timber columns with a dimension of 0.12 m × 0.06 m, planked with oriented strand boards with a thickness of 12 mm.

State 3 examines the CLT slab with drywall ceiling and added floating floor construction, which consists of the cement screed, the footfall sound insulation and the elastic bonded fill. The cross-section of the floor system is depicted in Fig. 4, the photo on the right of Fig. 2 illustrates the condition of the floor system after completion.

3. Methods

The test object was dynamically excited in all three construction states with the reaction masses of an electrodynamic long-stroke oscillator, type APS 400, driven by a power amplifier, type APS 145, with attached reaction masses, type APS 0412, and a dynamic active mass of 35 kg. In these tests, the shaker was fixed to the floor, as was the case in many previous vibration tests, see e.g. [29,30]. In all

Fig. 2. Test object in state 1 (left) and state 3 (right).

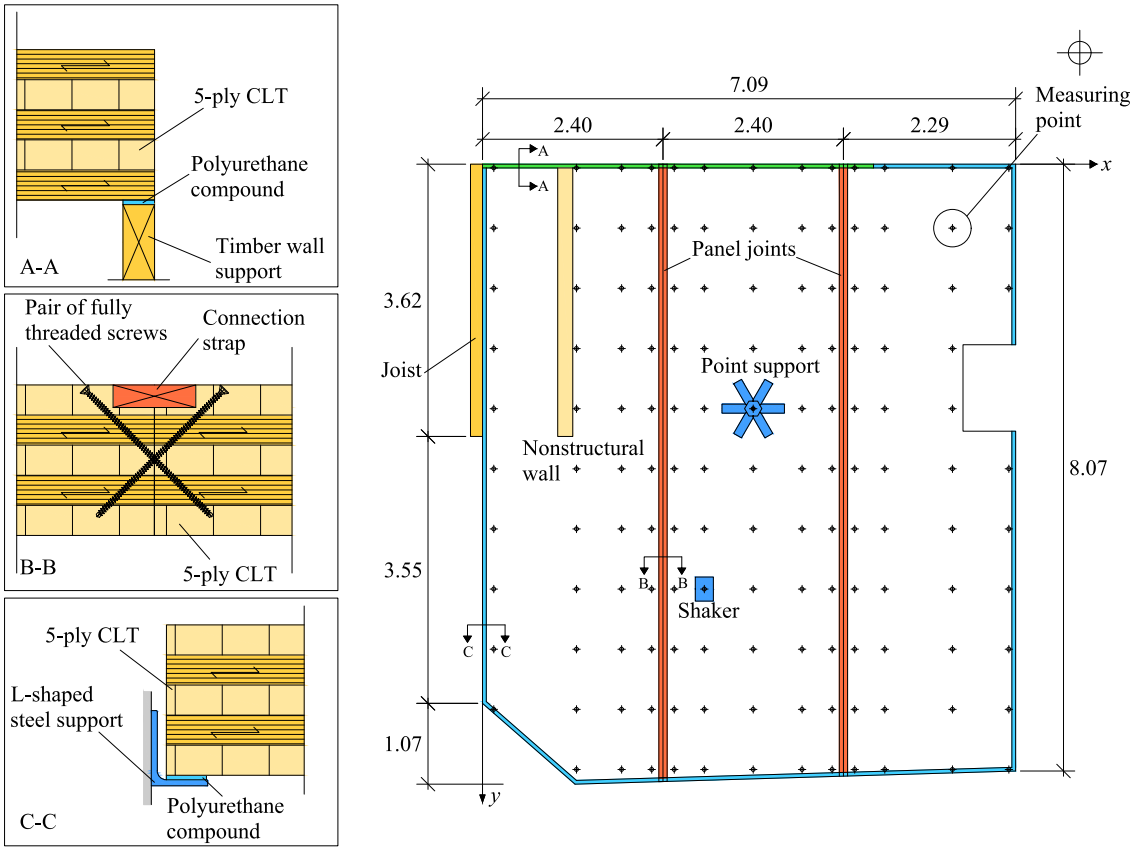

Fig. 3. Floor plan of the CLT slab, boundary conditions and construction details.

construction states, a linear sweep (chirp) with an initial signal ramp and a final signal decay period of 10 s each served as the excitation signal. In state 1, a sweep from 10 to 80 Hz in 220 s, in state 2 a sweep from 7 to 60 Hz in 220 s and in state 3 a sweep from 6 to 60 Hz in 180 s were performed, each repeated three times. Prior to the experiments, the input voltage signal at the power amplifier was iteratively adjusted so that the power spectral density (PSD) of the excitation acceleration (measured at the oscillating mass of the shaker) is constant in the frequency range considered. Fig. 5 shows the PSD for a single test in each of the states. Since the actual gain level had to be manually adjusted at the power amplifier, the amplitudes of the PSDs vary slightly between the three states, which is also reflected in the RMS values $\ddot{x}_{\mathrm{RMS,St}j}$ $(j = 1, \ldots, 3)$ of 0.475 g, 0.558 g and 0.327 g, respectively, for states 1 to 3. Note that the applied force on the CLT slab is assumed as the recorded acceleration at the oscillating mass times the mass of the attached reaction masses, since it is not possible to directly measure the force in this configuration.

The dynamic response was recorded with piezoelectric accelerometers, type Brüel&Kjær 4508 B, powered by a conditioning amplifier, type Brüel&Kjær 2694. A National Instruments cDAQ system with NI 9234 A/D converter modules controlled by a MATLAB program was used for data acquisition. The dynamic response in states 1 and 2 was recorded at 140 measuring points on the upper surface of the CLT slab.

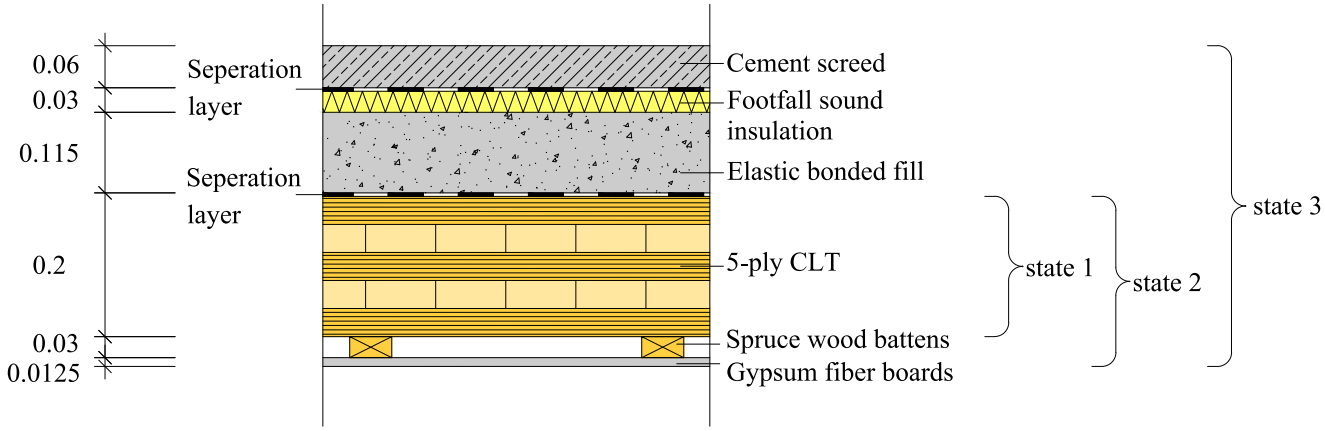

Fig. 4. Cross-section of the considered floor construction after completion.

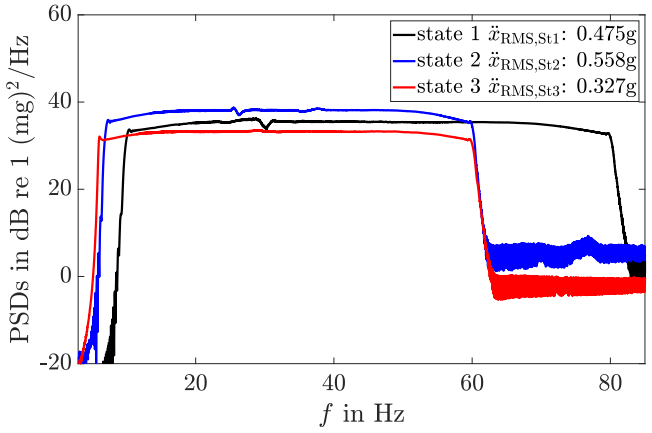

Fig. 5. PSD of the acceleration of the oscillating shaker mass for each state; corresponding RMS value specified in the legend.

The measurement grid for both states is shown in Fig. 3. In the x-direction, the grid is refined near the two panel joints to capture local effects, while in the y-direction the grid is regular. Since only eleven accelerometers were available, a total of 13 measurements had to be carried out to record the vibration response at all measuring points. For the measurements in state 3, a coarser regular grid of 86 measurement points was used, with sensor spacings of 1.0 m and 0.8 m in the x- and y-direction, respectively. Eight measurements were taken to record the response of the completed floor system on the surface of the floating screed.

For each construction state, the modal parameters, i.e. natural frequencies, damping ratios and mode shapes, were identified by two different system identification methods. In particular, the LSCE (Least Squares Complex Exponential) method in the time domain [31], which is widely used and implemented in MATLAB [32], and the LSCF (Least Squares Complex Frequency) method [33], which operates in the frequency domain, were applied to estimate the modal parameters of the prevailing single input–multiple output system [34] in each construction state. Although the two methods should yield the same structural poles for the measured system, the modal properties identified by the two methods may vary slightly. Stabilization diagrams were used to distinguish physical modes (referred to as poles) from mathematical poles [31]. A more detailed description of the system identification procedures can be found, for instance, in [31,34,35].

Subsequently, the outcomes of that method were used, which were identified as stable modes in the stabilization diagrams [35], and furthermore, the synthetic FRFs matched the experimental counterparts. Regardless of the model order chosen, physical poles appear to be stable, while mathematical poles, which try to model the noise in the model, change with an increasing model order. A pole is considered stable (denoted by P_{st}) if the relative changes in the ith natural frequency Δf_i^{EMA} and the ith damping ratio $\Delta\zeta_i$ between two model orders $m-1$ and m are within the following defined limits,

$$\Delta f_i^{EMA} = \frac{\left| f_{i(m-1)}^{EMA} - f_{i(m)}^{EMA} \right|}{f_{i(m-1)}^{EMA}} 100\% \quad \leq 1\% \quad \text{and}$$
$$\Delta\zeta_i = \frac{\left| \zeta_{i(m-1)} - \zeta_{i(m)} \right|}{\zeta_{i(m-1)}} 100\% \quad \leq 10\% \tag{1}$$

If one criterion in Eq. (1) is not met, the pole is identified as new pole, denoted as P_{new}. For the mode to be considered stable (denoted $Mode_{st}$), another criterion must be met,

$$\Delta\phi_i = \text{MAC}(\text{Re}(\{\phi\}_{i(m-1)}), \text{Re}(\{\phi\}_{i(m)})) \quad \geq 0.95 \tag{2}$$

In Eq. (2), the real parts, Re, of the ith mode shape vector, $\{\phi\}_i$, are compared between two model orders by computing the ith value of the modal assurance criterion (MAC), $\Delta\phi_i$ [36]. Note that the MAC is defined for complex vectors. However, since only the real parts of the experimental identified mode shapes can be matched to the numerical ones in the optimization procedure, only the real parts are compared when defining a stable mode. To find out whether the identified mode is complex, the mean phase correlation (MPC) as defined in [37] is used. A value close to unity means that the mode is real, while a lower value indicates a non-negligible imaginary part.

3.1. Finite element models

A finite element (FE) model was created in the FE software ABAQUS [38] for each construction state of the floor structure considered. The natural frequencies and mode shapes determined with this model were then validated with the experimental results. In these models, the CLT slab is discretized with four-node shell elements of type S4 with full numerical integration. First-order shear deformation theory (FSDT) [39] is employed as the kinematic assumption, which has been shown to be sufficiently accurate in the desired frequency range, provided the shear correction factors are chosen appropriately [40]. In the present study, the shear correction factors proposed in [41] for orthotropic laminates are used. The constitutive relations are implemented in the FE model using the general shell stiffness matrix, where the components of the strain stiffness matrix, the bending stiffness matrix and the shear stiffness matrix are defined according to [39]. The panel joints are modeled with connector elements [38] and have a variable bending stiffness along the joint. With a structured mesh in the vicinity of the

panel joints, rotational stiffnesses can be assigned to these connector elements, each connecting a pair of nodes of two adjacent panels.

The point support is idealized as a single node coupled to the nodes of the shell elements in the area of the steel connector, limiting the movement of these elements to that of the single node. By positioning the node below the middle surface of the shell model, some rotational stiffness is added to the point support [18]. In addition, the vertical flexibility of the support column is taken into account by a linear elastic spring. The horizontal flange of the steel profile (see Fig. 3), on which the slab partially rests, is represented in the model as a cantilever, which is discretized with shell elements. In that manner, the flexibility of the steel profile is taken into account. The joist supporting the upper left part of the slab is modeled with beam elements, and the part of the slab resting on a wall is elastically bedded in the model. The soundproofing polyurethane compound, which separates the CLT slab from the supports, is discretized with continuum elements of type C3D8, using the hyperelastic material model of Arruda–Boyce [38,42]. Since this constitutive law is nonlinear, a static computation under the impact of the gravity loads must be carried out prior to the FE modal analysis. At the stress level from this static computation, the material behavior is linearized, which is then implemented in the FE model for the modal analysis. The gravity forces are different in each construction state investigated and therefore the support stiffness in reality and in the model is also different for the three construction states.

As will be shown, the shaker interacts with the floor structure in the frequency range considered. Therefore, the shaker is assumed to be a spring–mass system in the FE model.

The FE model of the floor system in construction state 1 has 14,459 elements and 91,149 degrees of freedom. On this basis, the FE models for the floor system in states 2 and 3 are developed.

The gypsum fiber boards added in state 2 are modeled as a homogeneous, isotropic board with shell elements of type S4, the spruce wood battens with beam elements of type B31. The nonstructural wall is considered by distributing its effective mass evenly over its base dimensions. The resulting FE model for state 2 consists of 25,993 elements and has 161,361 degrees of freedom.

In the FE model of the test object in state 3, both the elastic bonded fill and the footfall sound insulation are discretized with continuum elements of type C3D8, while the floating cement screed is described with shell elements of type S4, resulting in a model with 134,210 elements and 586,713 degrees of freedom.

3.2. Model updating

From this description it is apparent that a relatively large number of parameters must be defined in the FE model, both in terms of material properties and boundary conditions. Some of these parameters are not or only insufficiently known. These must be determined in a two-stage model update procedure [43], as shown in Fig. 6. In a model update procedure, the parameters to be optimized are adapted until the results of the numerical model match the results from the measurements with sufficient accuracy. In the first step, the modal properties of the FE models are computed for states 1 and 2, with initial parameters taken from the literature where available. The natural frequencies and mode shapes obtained with the FE models are fed into an optimization procedure in MATLAB, which is based on the Nelder–Mead algorithm and implemented in the MATLAB function *fminsearch* [32]. The sums of the mean errors of the natural frequencies ϵ_{EF} and the sum of mode shapes ϵ_{MS} from the FE models and from the measurements are used as the objective functions for the optimization,

$$\epsilon_{EF} = \frac{1}{n}\sum_{i=1}^{n}\frac{|f_i^{\mathrm{FEM}} - f_i^{\mathrm{EMA}}|}{f_i^{\mathrm{EMA}}}, \qquad \epsilon_{MS} = \frac{1}{n}\sum_{i=1}^{n}\left[1 - \mathrm{MAC}\left(\{\phi\}_i^{\mathrm{FEM}}, \mathrm{Re}\left(\{\phi\}_i^{\mathrm{EMA}}\right)\right)\right] \tag{3}$$

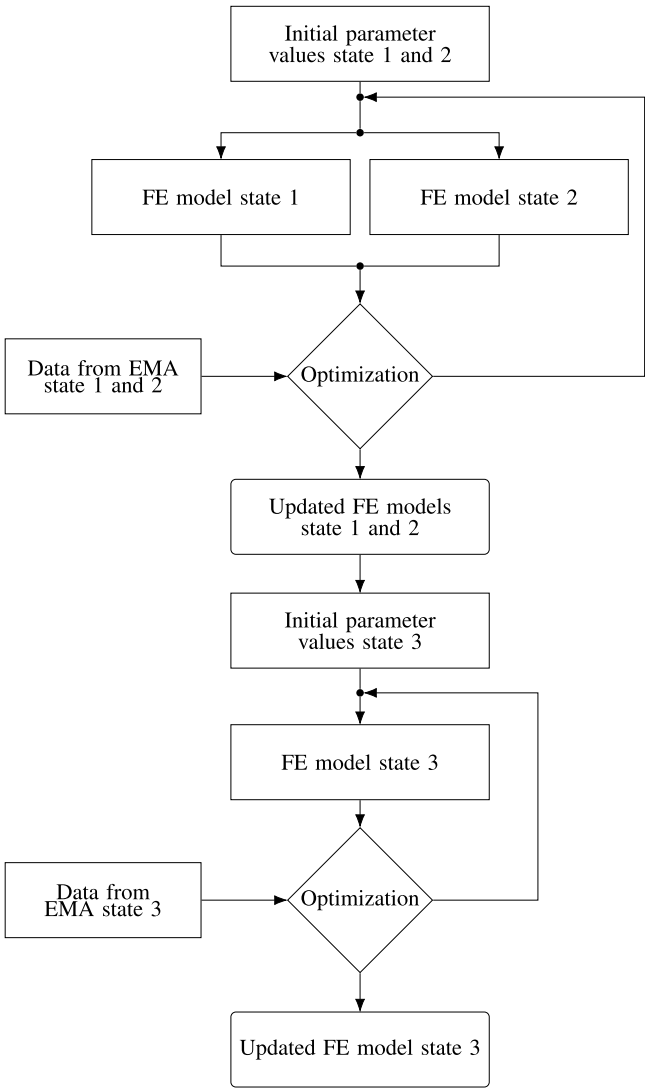

Fig. 6. Model updating procedure.

In this equation, f_i^{FEM} is the ith natural frequency computed numerically, f_i^{EMA} is the ith natural frequency determined from the measured data, and n is the number of modes considered in the updating procedure. $\mathrm{MAC}\left(\{\phi\}_i^{\mathrm{FEM}}, \mathrm{Re}\left(\{\phi\}_i^{\mathrm{EMA}}\right)\right)$ is the MAC value between the ith computed mode shape, $\{\phi\}_i^{\mathrm{FEM}}$, and the real part of the ith experimentally identified mode shape, $\mathrm{Re}\left(\{\phi\}_i^{\mathrm{EMA}}\right)$.

The optimized FE models of states 1 and 2 serve as the basis for the FE model of state 3. In a second optimization step, the parameters for the added components of the floating screed are determined with the same procedure, while the parameters of the CLT slab, the drywall ceiling and the supports are used as found in the first optimization step.

4. Identification of modal properties

This section presents the results of the experimental modal analysis for the three construction states of the floor system. In the stabilization diagrams presented, dots indicate new poles, cross-shaped markers indicate stable poles and squared markers indicate stable modes, according to the criteria defined in Section 3. In addition, the mean value of the frequency response functions (FRFs) for all measuring points is represented by a solid line to facilitate the distinction between physical and non-physical poles.

Table 1
Experimentally identified natural frequencies $f_{i,\mathrm{St}j}^{\mathrm{EMA}}$, damping ratios $\zeta_{i,\mathrm{St}j}$ and mean phase correlations $\mathrm{MPC}_{i,\mathrm{St}j}$ of the CLT slab in three construction states (construction states denoted with subscript $j = 1, 2, 3$; modal parameters denoted with subscript $i = 1, \ldots, 6$.

Mode (i)	$f_{i,\mathrm{St1}}^{\mathrm{EMA}}$ [Hz]	$\zeta_{i,\mathrm{St1}}$ [%]	$\mathrm{MPC}_{i,\mathrm{St1}}$ [–]	$f_{i,\mathrm{St2}}^{\mathrm{EMA}}$ [Hz]	$\zeta_{i,\mathrm{St2}}$ [%]	$\mathrm{MPC}_{i,\mathrm{St2}}$ [–]	$f_{i,\mathrm{St3}}^{\mathrm{EMA}}$ [Hz]	$\zeta_{i,\mathrm{St3}}$ [%]	$\mathrm{MPC}_{i,\mathrm{St3}}$ [–]
1	12.78	5.07	0.91	12.02	8.14	0.90	10.68	2.08	0.98
2	13.92	3.48	0.76	14.31	5.68	0.89	13.74	2.68	0.94
3	16.32	4.81	0.89	14.78	5.06	0.91	15.24	2.12	0.65
4	23.55	4.57	0.80	16.70	1.90	0.87	20.16	3.60	0.85
5	25.22	3.79	0.88	23.13	8.13	0.61	–	–	–
6	–	–	–	25.45	4.38	0.87	–	–	–

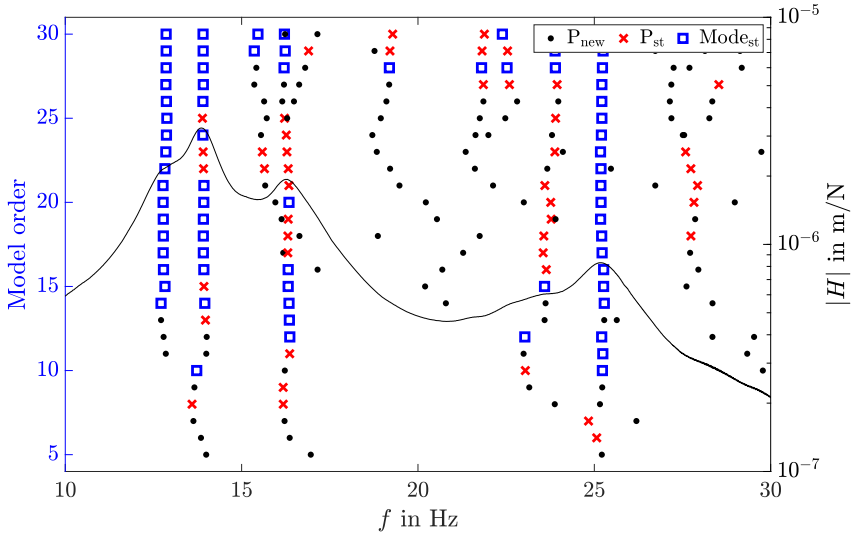

Fig. 7. Stabilization diagram and mean FRF for the CLT slab in state 1 resulting from the LSCE method.

4.1. State 1

Fig. 7 shows the stabilization diagram of the acceleration response recorded on the top of the CLT slab at state 1 in a frequency range from 10 to 30 Hz. Considering the mean value of the FRFs, at least five distinct resonance peaks can be seen, but with increasing frequency the peaks are no longer clearly identifiable. From a model order of 11, five poles can be found between 10 and 30 Hz, which are stable at a model order of 15. For higher frequencies, no stable modes are present.

The physical modes identified from the stabilization diagram using the LSCE method with their corresponding natural frequencies, damping ratios and mean phase correlations (MPCs) are listed in Table 1. The fundamental frequency is 12.78 Hz, and the largest identified natural frequency is 25.22 Hz. According to the modal parameter estimation, the damping ratios $\zeta_{i,\mathrm{St1}}$ vary between 3.48 and 5.07%, with the largest damping ratio associated with the fundamental mode. The MPC values of these modes range from 0.76 to 0.91, indicating that the modes are not purely real but moderately complex.

Fig. 8 depicts the real part of the mode shapes. As observed, the mode shape of the fundamental mode (natural frequency 12.78 Hz) has the largest amplitudes near the shaker position, cf. Fig. 3. The second mode has a frequency of 13.92 Hz and the corresponding mode shape is a bending mode with a clear nodal line in the y-direction. The third mode identified at 16.32 Hz, like the first mode shape, has no nodal line. At first glance, it seems unreasonable that two modes occur without a nodal line. However, in Section 4.4 a rationale for this is provided. The fourth mode is a bending mode with a nodal line approximately in the x-direction and has a natural frequency of 23.55 Hz. The last identified mode with a natural frequency of 25.22 Hz is a bending mode with two nodal lines.

4.2. State 2

For the EMA of the floor system in state 2, the stabilization diagram is shown in Fig. 9. The mean FRF, also shown in this figure in a frequency range between 10 and 30 Hz, has six resonance peaks at frequencies with stable modes. The identified modal parameters, i.e. natural frequencies, damping ratios, of state 2 resulting from the LSCF method and MPC values are listed in Table 1. The damping ratios $\zeta_{i,\mathrm{St2}}$ ($i = 1, \ldots, 6$) range from 1.90 to 8.14%, with the largest value again observed for the first mode. According to Table 1, the MPC values for the six modes range from 0.61 to 0.91. The fundamental frequency of the CLT slab in state 2 is 12.02 Hz. The corresponding mode shape shown in Fig. 10 correlates with the corresponding mode shape in state 1. The mode shapes of the second and third identified modes with natural frequencies of 14.31 Hz and 14.78 Hz, respectively, are similar to the first one. This unexpected result is discussed further in Section 4.4. The mode shapes of the fourth, fifth and sixth identified modes with natural frequencies of 16.70 Hz, 23.13 Hz and 25.45 Hz, respectively, are similar to modes 2, 4 and 5 in state 1. The natural frequency of the fourth mode with 16.7 Hz is clearly larger than the corresponding mode with the same mode shape (mode 2) in state 1 with 13.92 Hz. In this mode, installing the drywall ceiling as well as the partition wall yields an increase of this natural frequency. The natural frequencies of the other corresponding modes are virtually not affected by the structural changes between state 1 and 2.

4.3. State 3

The stabilization diagram for the EMA in state 3 is shown in Fig. 11. The mean FRF also displayed in this figure shows four well separated resonance peaks in the considered frequency range between 10 Hz and 30 Hz. The identified natural frequencies and damping ratios, estimated

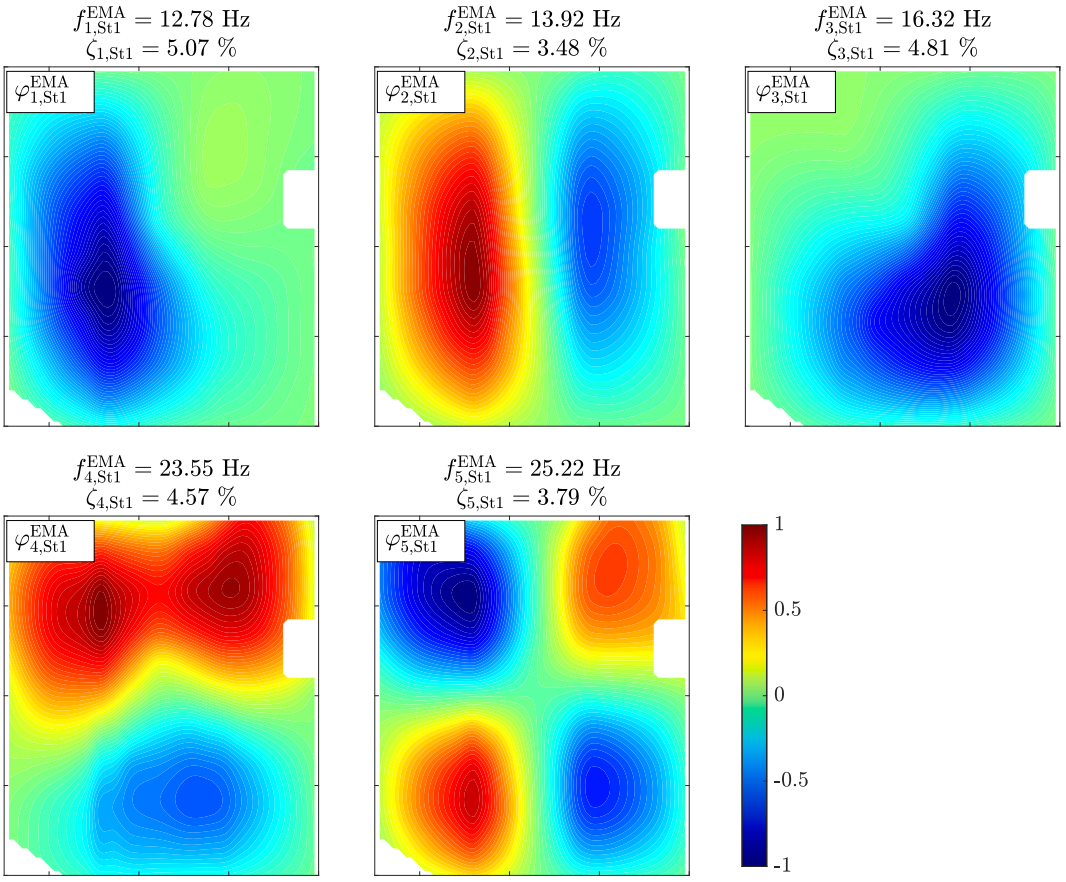

Fig. 8. Identified modes 1 to 5 of the CLT slab in state 1.

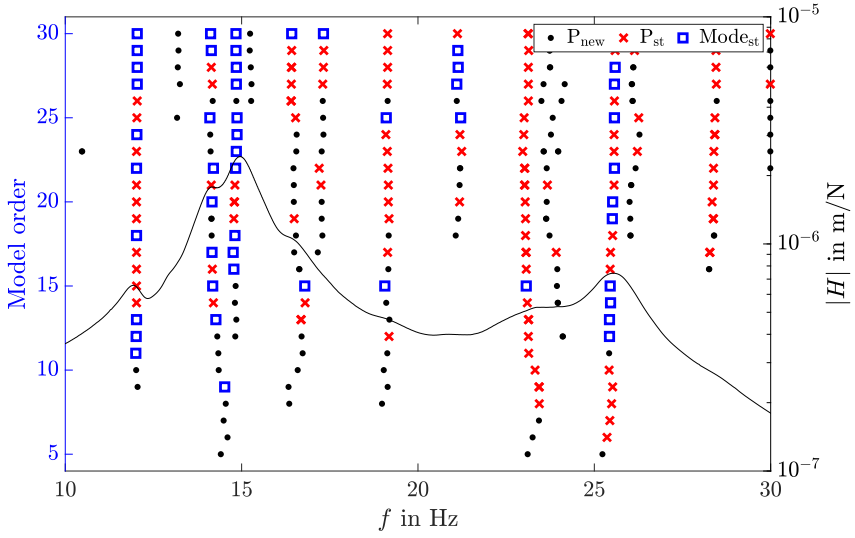

Fig. 9. Stabilization diagram and mean FRF for the CLT slab in state 2 resulting from the LSCF method.

with the LSCE method, and MPC values of state 3 are listed in Table 1. Compared to states 1 and 2, the natural frequencies have shifted to lower values due to the mass of the added floating screed. Thus, the fundamental frequency in state 3 is 10.68 Hz compared to 12.78 Hz in state 1 and 12.02 Hz in state 2.

Interestingly, the damping coefficients $\zeta_{i,\mathrm{St3}}$ in state 3 are also considerably smaller than in the previous investigated states. The reason for this is attributed to the drastic change in mass of the floor system in state 3. In state 1, the damping values range from 3.48% to 5.07%, while the largest damping value of state 2 is found to be 8.14% in the fundamental mode. In this raw state, the floor system has gaps between interacting structural elements and the contact is most likely not fully developed, for instance in the two panel joints, resulting in greater friction and thus larger damping values. In state 2, when the drywall ceiling is in place and the partition wall is erected, these effects are amplified, which explains the increase in damping values compared to state 1. In state 3, the mass of the system is more than tripled, taking into account the bonded fill and screed, resulting in closed joints and

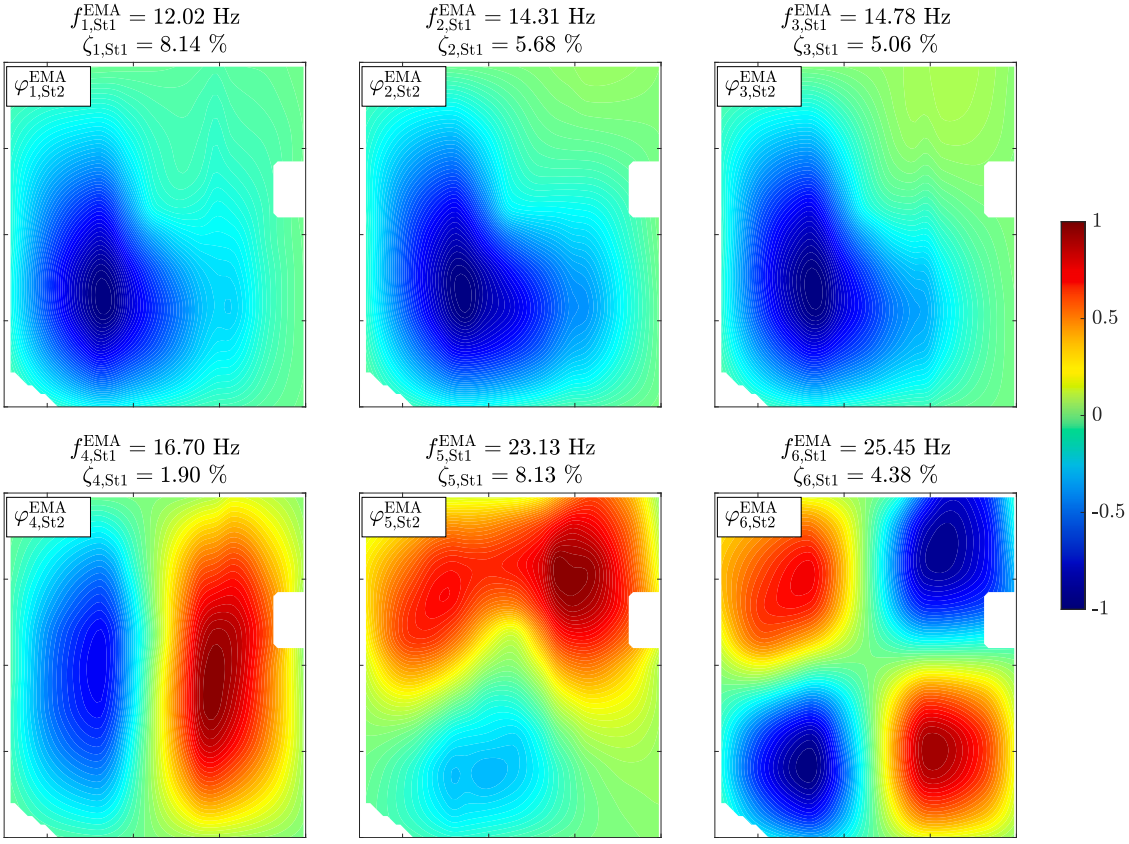

Fig. 10. Identified modes 1 to 6 of the CLT slab in state 2.

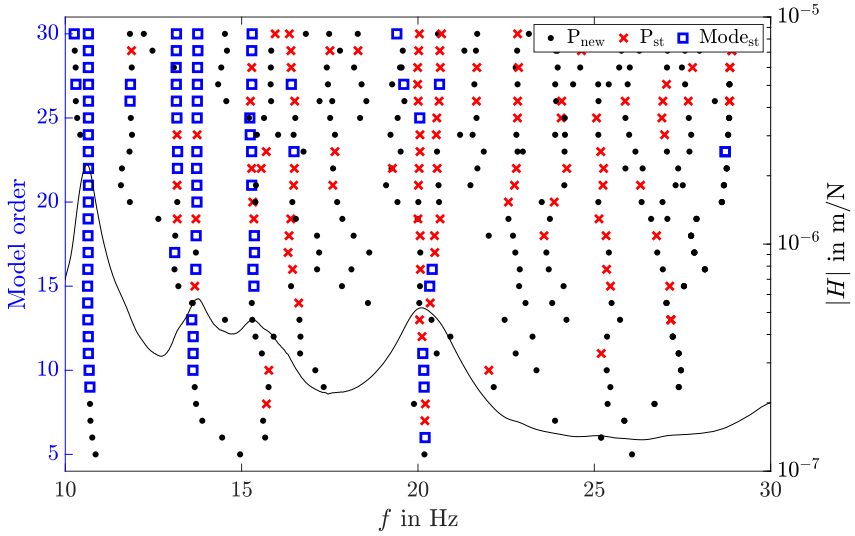

Fig. 11. Stabilization diagram and mean FRF for the floor system in state 3 resulting from the LSCE method.

cracks and a fully developed contact between the components, and thus less energy is dissipated by friction, leading to smaller damping values. The damping of the fundamental mode is smallest at 2.08%, while the largest damping value occurs in the fourth vibration mode at 3.60%.

The MPC values range from 0.98 to 0.65, with the lowest value associated with the third mode, which is consistent with the results in state 2.

The mode shapes shown in Fig. 12 are similar to the first four mode shapes of a simply supported plate, i.e. the influence of point support is hardly noticeable in state 3. It seems that this point support has only some effect on the fundamental mode. In contrast to the previous construction states, only one mode (i.e. the fundamental mode) without nodal line occurs here.

4.4. Identified modes due to shaker–structure interaction

Assuming a linear elastic system, the mode shapes of the floor construction should be unique. However, this is not the case for some of the identified modes (modes 1 and 3 in state 1, modes 1 to 3 in state 2). To quantify the correlation of the mode shape vectors, the MAC values

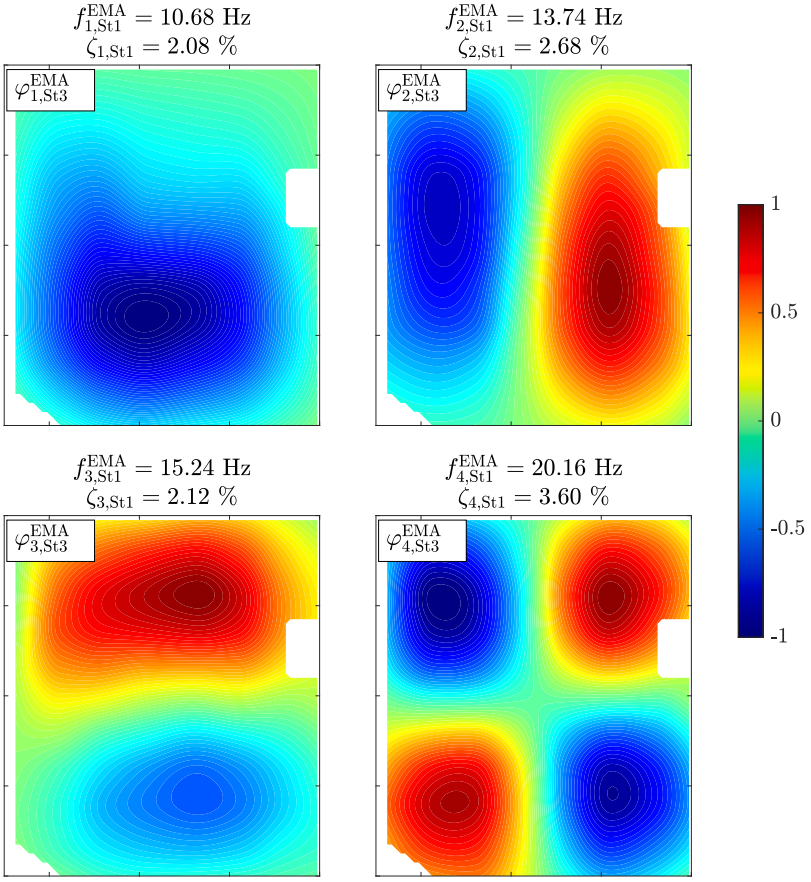

Fig. 12. Identified modes 1 to 4 of the floor system in state 3.

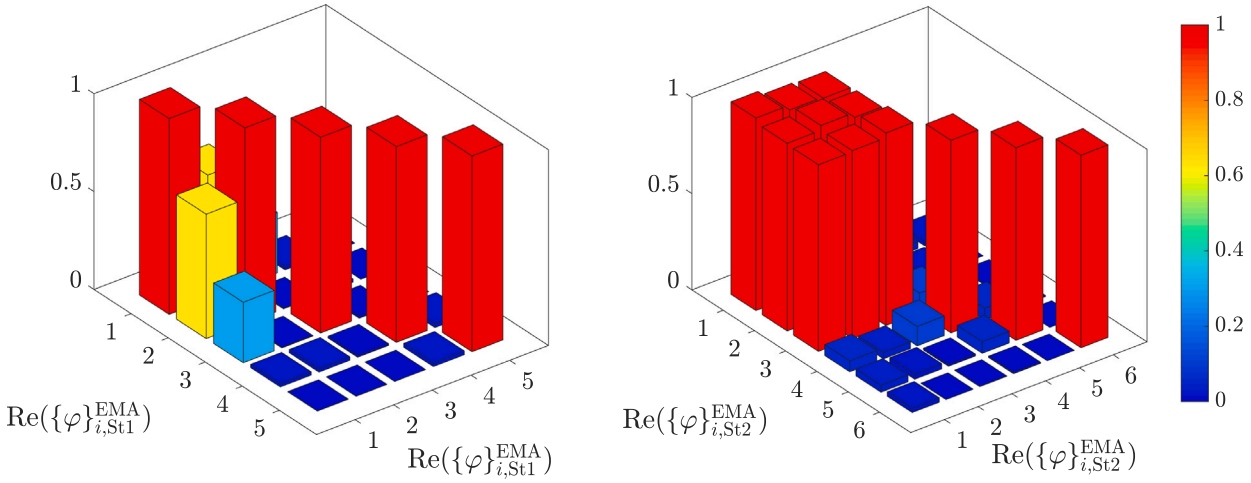

Fig. 13. Visualization of the auto-MAC matrix of the mode shapes from EMA in state 1 (left) and state 2 (right).

are computed, particularly the auto-MAC matrix [34]. In Fig. 13 this matrix is visualized for the identified modes of state 1 (left) and state 2 (right). As observed, the off-diagonal terms in the auto-MAC matrices for the first three modes are not negligible, which is already evident from the visual assessment of Figs. 8 and 10.

In [36] a number of possible reasons are given for why similar mode shapes with different corresponding natural frequencies (and thus off-diagonal auto-MAC values) are identified during system identification. One reason may be contamination of the measured data with noise, resulting in random noise vectors or vectors associated with unphysical poles. This is ruled out due to the relatively large acceleration signal levels in the measured data, compare Fig. 5, and the thorough examination of the FRFs and pole estimates.

Another reason given is that the modal vectors are incomplete because the response was measured at too few points. At first glance, this justification does not seem to apply either, since a dense measurement grid has been placed over the panel. After further considerations and calculations, however, it becomes apparent that in fact the system (and thus the modal vectors) has only been incompletely recorded, since on the one hand the shaker, which itself represents a vibrating system with a natural frequency close to the fundamental frequency of the slab, has not been taken into account and on the other hand no measurements

have been taken in state 2 on the drywall ceiling, which also interacts dynamically with the CLT panel. This explanation is supported by the fact that the majority of the affected mode shapes have their largest modal amplitudes at the position of the shaker. Furthermore, as outlined in Section 3, the applied force of the shaker on the test object cannot be directly measured by a force transducer. Therefore, the resulting force on the slab is assumed equal to the acceleration of the oscillating reaction masses, which is recorded during the tests, times mass. This is a correct assumption if the shaker can be rigidly clamped to the CLT slab. However, since this is not possible, the actual applied force is unknown and a disturbance in terms of e.g. rocking of the shaker can occur, leading to a resonance peak in the experimental data. With the additional mass due to the floor construction it is assumed that the interaction of the slab with the shaker and the drywall ceiling is negligible in state 3, and thus no odd modes have been identified.

Another possibility for the observed large off-diagonal auto-MAC values may be non-linear effects, in particular due to an opening and closing of contact zones in the two panel joints during the dynamic tests. Considering that natural frequencies of modes 2 and 3 of state 2 are closely spaced at 14.31 Hz and 14.78 Hz, respectively, and the accelerations of the vibrating shaker mass were significantly larger in state 2 than in the other two states, see Fig. 5, nonlinear effects are amplified and two apparently identical mode shapes are identified at two adjacent natural frequencies. This will be further elaborated in the sections concerning the numerical simulations.

5. Numerical parameter identification

The corresponding FE models should accurately represent the structure at all construction states with as few parameters as possible to ensure that the updated parameters can be considered as globally optimal. In the following, the parameters and their corresponding initial values used in the two-step model updating procedure described in Section 3.2 are presented.

It is assumed that the individual wood layers of the CLT have a linear elastic orthotropic material behavior. According to the applicable timber construction standards, a distinction is made between the material parameters parallel to the grain and perpendicular to the grain. The initially chosen parameters for spruce of strength class C24 are the modulus of elasticity $E_1 = 11{,}000$ MPa, the shear modulus $G_{12} = G_{13} = 690$ MPa and the rolling shear modulus $G_{23} = 56$ MPa, which are taken from [26,44]. The moduli of elasticity perpendicular to the grain are assumed to depend on the parallel value and are therefore set to $E_2 = E_3 = E_1/30$. To reduce the number of parameters to be optimized, the elasticity coefficients E_1, G_{12} and G_{23} are considered to be dependent on each other. Therefore, a single variable s_M is used as a linear scaling factor for these properties in the optimization procedure. Preliminary studies have shown that the modal parameters are not sensitive to the values of the Poisson ratios. Thus, the Poisson ratios are set to a fixed value of $\nu_{12} = \nu_{13} = \nu_{23} = 0.4$. A value of $\rho_{CLT} = 490\,\mathrm{kg/m^3}$ is chosen as the initial value for the density of the CLT slab.

As far as the authors are aware, there are no generally valid data for estimating the rotational stiffness of the joints between the CLT panels. In order to obtain a realistic value of this rotational stiffness, a simply supported CLT beam under a constant line load q is considered in a preliminary study, which is composed of two parts that are connected in the middle of the beam by a pair of fully threaded screws — just like the panels of the floor construction under consideration. For this beam, on the one hand, a three-dimensional (3D) FE model of continuum elements (C3D8) is created (Fig. 14(a)), in which the screws are taken into account by embedded elements as well as the contact area in the beam center by contact conditions. By incrementally increasing the line load, the displacement at midspan is computed and presented in the form of a load–displacement diagram. In a second modeling approach, this structure is simplified as a Timoshenko beam (Fig. 14(b)), where a rotational spring with stiffness γ_{UB} is placed in the beam center. By fitting the static response of the beam model to the load–displacement curve of the 3D model the (linearized) rotational spring stiffness γ_{UB} sought is obtained.

In Fig. 15 the load–displacement curve of the 3D continuum model is shown with the solid black line and that of the Timoshenko beam model with a dashed black line. In addition, the blue lines in this figure represent the global bending stiffness of both modeling variants, denoted by k_b, as a function of the midspan displacement u, which corresponds to the slope of the load–displacement curves. Since in the 3D model the contact between the two beam elements is only gradually established in the first load steps, the load–displacement curve is nonlinear in this range. Accordingly, the bending stiffness also increases nonlinearly. Only after full contact is reached, this curve becomes linear and the bending stiffness is constant with $k_b = 260$ kN/m. The nonlinear behavior cannot be reproduced with a linear beam model. In contrast, the linear range is perfectly reproduced by the rotational spring stiffness per unit length $\gamma_{UB} = 1.5$ MNm/(rad m). This value can be considered as an upper limit for the rotational stiffness of the panel joints. However, if the contact between the panels is not yet fully established, the equivalent rotational stiffness is smaller. Since the gravity loads increase with each construction state, it can be assumed that the equivalent bending stiffness of the panel joints also increases with each construction state. In the FE models of the slab under consideration, a rotational spring with a variable stiffness parameter is therefore introduced at the location of each connection, which is adjusted for each construction state by means of model updating. To determine the shear stiffness of the joint, opposing loads on the respective beam sections are also considered and a vertical spring stiffness is estimated using the same method as for the rotational spring stiffness. It turned out that the obtained vertical spring stiffness has no effect on the modal properties compared to a rigid connection and is therefore neglected in the FE model.

In the FE model, three parameters describe the flexibility of the supports of the CLT slab, where two parameters are considered in the model updating procedure. All parameters used in the optimization procedure are listed in Table 3. The first optimization parameter is the stiffness k_c of the spring, which represents the longitudinal stiffness of the point support. The initial value of this stiffness follows from the relation $k_c = E_1 A/l$ to $k_c = 125.7$ MN/m, where A is the cross-sectional area of the column on the lower floor with the diameter of 0.2 m, the length $l = 3.0$ m and the estimated initial modulus of elasticity in parallel direction $E_1 = 12000$ MPa. The second optimization parameter is the equivalent shear modulus for the hyperelastic material of the polyurethane compound between the CLT slab and the L-shaped steel support, whose initial value of $\mu = 1.0\ \mathrm{MN/m^2}$ was identified from the manufacturer's stress–strain curve [45]. From μ and the Poisson's ratio, which is set at $\nu = 0.49$, the corresponding bulk modulus can be determined [38]. The modulus of elastic bedding in the boundary region supported by the wall is the third stiffness parameter. However, as a result of the preliminary numerical investigations, the parameter is not considered as optimization parameter, since the influence on the modal properties is negligible and therefore is set to a fixed value of $\bar{k}_w = 100\ \mathrm{MN/m^3}$.

For the spring–mass system, which models the disturbance of the shaker, the spring stiffness is unknown. Since the stiffness varies between each test due to the assembly and disassembly of the shaker for transport or different boundary conditions or due to different boundary conditions when the shaker is placed on the surface of the slab, a separate spring stiffness is introduced for each of the first two construction states. However, the initial value is chosen to be the same for both states with $k_{j,s} = 215$ kN/m ($j = 1, 2$), which corresponds to a natural frequency of the spring–mass system of 12.5 Hz.

The material parameters of the steel profiles, the joist, the wood battens and the gypsum fiber boards are not taken into account in the model updating procedure, as preliminary simulations have shown that they have only a minor influence on the dynamic behavior, provided

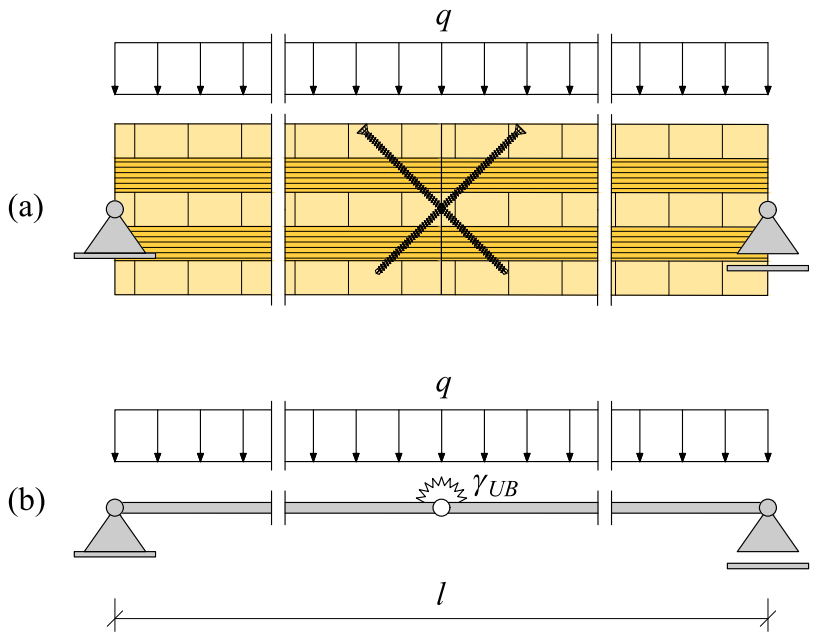

Fig. 14. (a) Continuum model and (b) corresponding beam model used to estimate the equivalent stiffness of the rotational springs representing the panel joints.

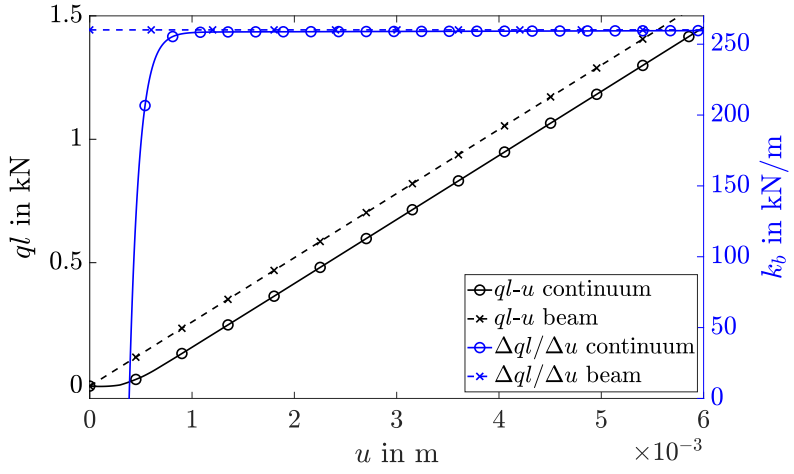

Fig. 15. Load–displacement diagram (black lines) and global stiffness (blue lines) of the models used to estimate the equivalent stiffness of the rotational springs representing the panel joints. (For interpretation of the references to color in this figure legend, the reader is referred to the web version of this article.)

that physically reasonable parameters are used. Note that although these parameters are not updated, the corresponding components are important for the model of state 2. The timber elements are modeled with the material parameters of spruce, which are introduced as initial material parameters for the individual wood layers of the CLT, the moduli of elasticity and the density for steel profiles are $E_s = 210,000$ MPa, $\rho_s = 7850$ kg/m^3 and $E_g = 3800$ MPa, $\rho_g = 1150$ kg/m^3, respectively, and for the gypsum fiber boards $E_g = 3800$ MPa, $\rho_g = 1150$ kg/m^3, respectively.

For the numerical simulation of the test object in state 3, the modulus of elasticity $E_{sc} = 22,000$ MPa and the density $\rho_{sc} = 2000$ kg/m^3 of the screed are considered as fixed values, while the screed thickness is a parameter to be optimized with initial value $d_e = 0.06$ m. Thus, indirectly both mass and stiffness of the screed are varied in the optimization.

The initial value of the dynamic stiffness modulus of the footfall sound insulation is set to $s_f = 12$ MN/m^3, which is a common value for timber floors. With the fixed thickness of 0.03 m, this gives the modulus of elasticity for the footfall sound insulation of $E_f = 0.36$ MPa as the initial value, which is another optimization parameter. The elastically bonded fill is characterized by two optimization parameters, the density (initially set to $\rho_{bf} = 1600$ kg/m^3) and the modulus of elasticity (initially one tenth of the cement screed, i.e. $E_{bf} = 2200$ MPa).

5.1. Sensitivity analysis

A sensitivity analysis is carried out to quantify the influence of every optimization parameter on the modal properties and subsequently to rule out parameters in the model updating process, which have only a minor influence on the outcome of the numerical computations. For state 1 and state 2, seven optimization parameters are considered each, while four parameters are varied in the optimization procedure in state 3. All parameters are summarized in Table 3.

From the seven parameters varied in the model updating procedure in state 1 and state 2, four parameters (the shear modulus of the polyurethane compound μ, the vertical flexibility of the point support k_c, the density of the CLT panels ρ_{CLT} and the scale factor for the stiffness parameters of the timber material s_M) affect the numerical results of the models for both states. The rotational spring stiffnesses

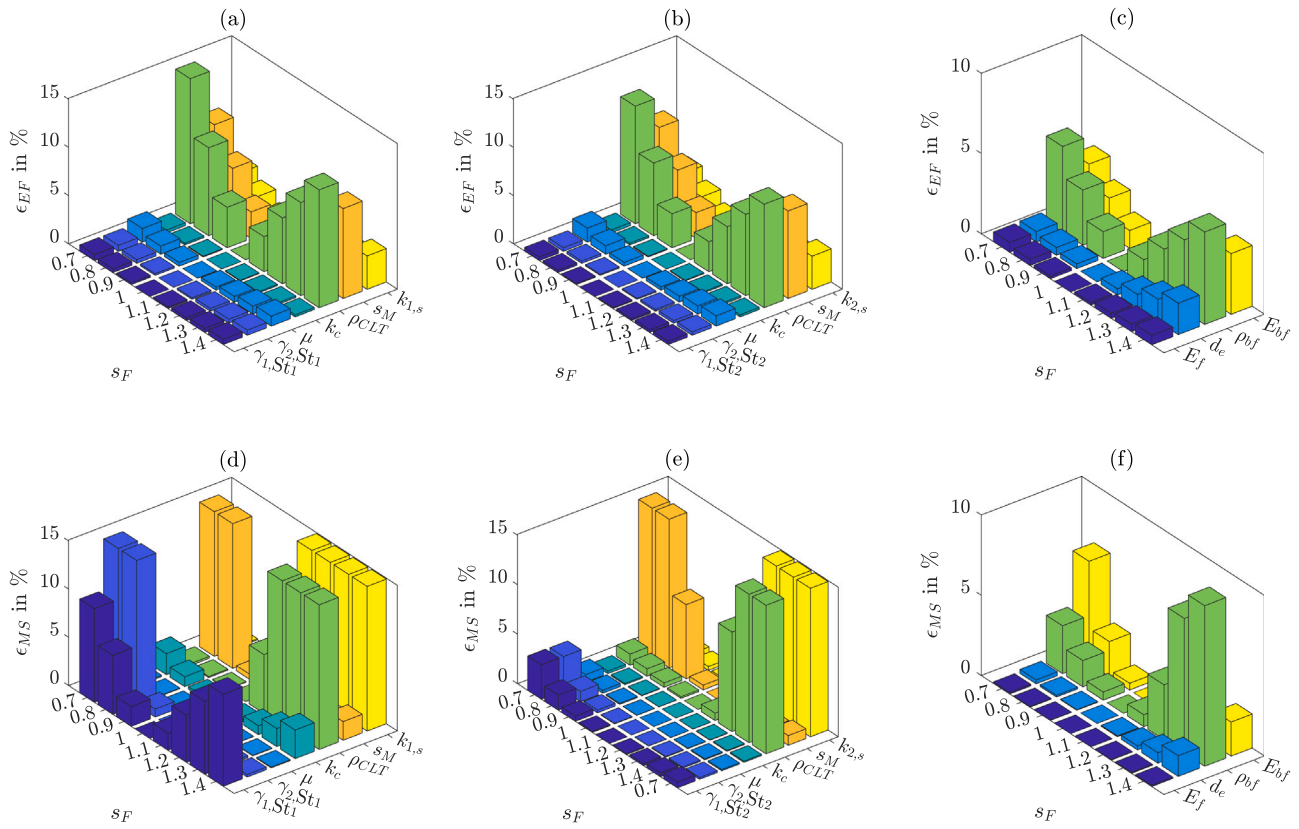

Fig. 16. (a)–(c): sum of the mean relative errors of the natural frequencies ϵ_{EF}, (d)–(f): sum of the mean mode shape errors ϵ_{MS}, for state 1 to state 3, respectively.

$\gamma_{1,\mathrm{St}j}$ and $\gamma_{2,\mathrm{St}j}$ as well as the stiffness of the spring–mass system of the shaker model $k_{j,s}$, with $j = 1, 2$, are different in each of the two states.

For state 1, the sum of the mean relative errors of the natural frequencies ϵ_{EF} and the sum of the mean mode shape errors ϵ_{MS}, defined in Eq. (3), are depicted in Fig. 16(a) and (d), respectively, for the initial parameters, which are multiplied by a scaling factor $s_F = 0.7, \ldots, 1.4$ sequentially, to evaluate the changes in natural frequency and mode shapes. The material parameters of the CLT elements, i.e. density ρ_{CLT} and the scale factor s_M, have the largest impact on the natural frequencies of the model. Naturally, the spring stiffness of the shaker-mass system affects the natural frequency of the mode that is identified due to shaker–structure interaction. Compared to the material parameters, the stiffness parameters corresponding to the boundary conditions of the system have a smaller but non-negligible impact on the natural frequencies, when comparing the sum of the mean relative errors (cf. Fig. 16(a)). These parameters considerably change the resulting mode shapes, which is depicted in Fig. 16(d).

Varying the optimization parameters of state 2, results in similar mean relative errors of the natural frequencies, as depicted in Fig. 16(b), compared to the results of state 1, while the mode shapes seem to be less affected by the boundary conditions (Fig. 16(e)). Since the material parameters and boundary conditions of the load-bearing structure are part of the model updating in state 1 and state 2, four parameters that affect the material parameters of the non load-bearing floor construction are varied in state 3. These are the modulus of elasticity of the footfall sound insulation E_f, the screed thickness d_e (which directly influences both mass and stiffness of the screed), the density ρ_{bf} as well as the modulus of elasticity E_{bf} of the bonded fill. In Fig. 16(c) the change in the natural frequencies is depicted, following the same sensitivity study. As can be seen, all parameters affect the natural frequencies, in particular the density and the modulus of elasticity of the bonded fill have the largest impact. Also the mode shapes are largely influenced by the parameters of the bonded fill (cf. Fig. 16(f)), while the density of the screed and the modulus of elasticity only have minor impact on the mode shapes. Note that the results of the sum of the mean errors of the mode shapes are truncated at 15% for state 1 and state 2 and at 10% for state 3 for visibility purposes. Results larger than these limits imply that by changing the parameter values, the sequence of mode shapes no longer matches those determined with the initial parameters.

5.2. State 1 and state 2

The FE models for state 1 and state 2 are updated in parallel according to the model updating procedure described in Section 3.2. In total, ten parameters are updated in this optimization step, as outlined in the previous paragraphs. This includes two rotational spring stiffnesses representing the slab joints for each state $\gamma_{1,\mathrm{St}j}$ and $\gamma_{2,\mathrm{St}j}$ ($j = 1, 2$ denoting the corresponding state), one spring stiffness representing the shaker flexibility for each state $k_{j,s}$, the point support spring stiffness k_c, the shear modulus of the hyperelastic polyurethane compound μ, the scaling factor for the elastic material parameters of the timber s_M and the density of the CLT slab ρ_{CLT}.

The updated parameter values are listed in Table 3. The rotational spring stiffnesses of the panel joints are given per unit length, since the stiffness of the discrete rotational springs used in the FE models is mesh dependent. As can be seen, the rotational stiffness increases significantly from state 1 to state 2. This is attributed to the fact that the mass increases in state 2 and thus the contact in the joints is more pronounced, as well as to the fact that installation of the drywall ceiling also increases the stiffness in the transversal direction. This increase is also evident in the measurement data when comparing the modal properties (natural frequencies and modes shapes) of state 1 and state 2. Mode 2 in state 1 is mainly dominated by the bending stiffness of the slab in transverse direction and the rotational stiffness of the joints. Since the bending stiffness of the CLT slab does not change, the

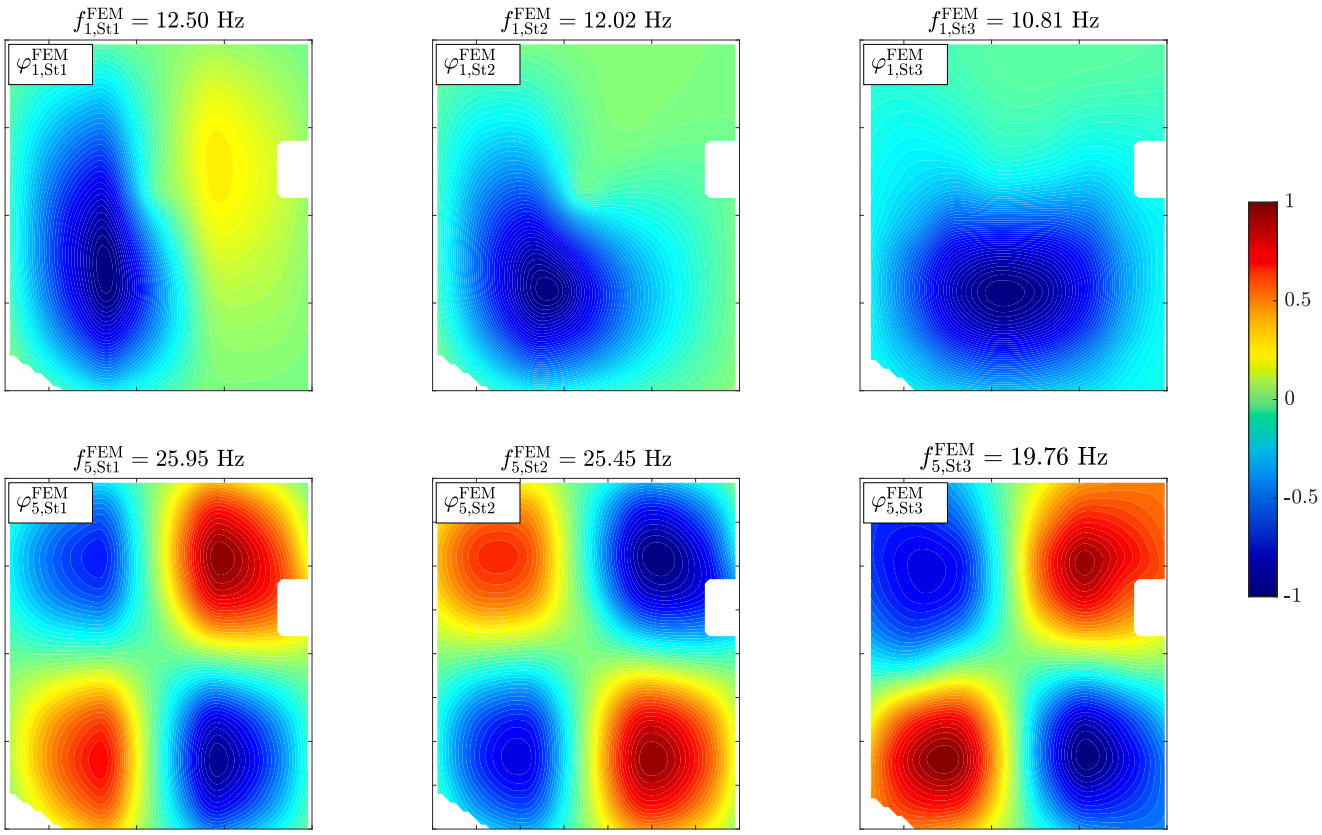

Fig. 17. Selected numerically identified mode shapes of state 1, 2 and 3.

increase in natural frequency from 13.92 Hz in state 1 to 16.70 Hz in state 2 (comparing the correlating mode shapes) must be to be due to a significant increase in rotational stiffness. Moreover, the left panel joint, cf. Fig. 3, has a higher rotational stiffness ($\gamma_{1,\mathrm{St}j}$) than the panel joint on the right hand side ($\gamma_{2,\mathrm{St}j}$).

The determined spring stiffness of the shaker model results in a natural frequency of the shaker of 13.30 Hz in state 1 and 12.42 Hz in state 2. This is consistent with the results of the EMA, where the first identified natural frequency in state 1 is larger than the first natural frequency in state 2. The difference in the shaker frequency is due to the fact that the shaker was disassembled for transport and reassembled on site before each measurement and the boundary conditions of the shaker attachment might vary.

The updated value of the point support stiffness increases compared to the initial assumption, while the shear modulus for the polyurethane compound decreases. The elastic parameters for spruce used to compute the slab stiffness increase by about 24%, i.e. $E_1 = 13,640$ MPa, $G_{12} = 855$ MPa and $G_{23} = 57$ MPa, while the density slightly decreases, i.e. $\rho_{CLT} = 464$ kg/m^3.

When the FE analysis is performed with these optimized parameters, the natural frequencies given in Table 2 are obtained. Also listed is the relative error between these numerically determined natural frequencies and the values from the EMA according to Eq. (3), which in state 1 is between 1.62 and 3.11%. The difference between the mode shapes from the FE analysis and the real part of the corresponding mode shapes from the EMA are evaluated by means of the cross-MAC matrix [34]. The resulting MAC values can be likewise found in Table 2. In state 1, the MAC values for the first four modes are close to 0.9, indicating a close correlation. The MAC value of the fifth mode of 0.82 could be due to the fact that higher modes are more prone to inaccurate grid positions of the sensors when recording the dynamic response of the slab.

In state 2, the relative error between the natural frequencies of the computational model and the EMA is in the range of 0.00% and 5.04% with a mean error of 1.87%. The MAC values range from 0.89 to 0.96, which is an excellent correlation with the experimentally identified modes. The visualized cross-MAC matrices in Fig. 18 show the same properties as the auto-MAC matrices in Fig. 13 with relatively large non-diagonal MAC values. In Fig. 17 the numerical identified mode shapes of mode 1 and 2 for states 1 and 2 are depicted. If one compares the numerically determined mode shapes with the correlating experimentally determined ones, see Figs. 8 and 10, one can also observe, as suggested by the MAC value, that the modes match very well. Note that when a shaker system with a single degree of freedom is used in the FE model, the first mode, which is identified as a mode due to the shaker–structure interaction, can be accurately identified numerically as well as in state 1. The closely spaced second and third mode cannot be reproduced in this linear model since the behavior is attributed to nonlinear effects of the panel joints, as outlined in Section 4.4. Therefore, only five of the six experimentally identified modes are considered in the MAC matrix.

5.3. State 3

The FE model for state 3 supplements the previously updated FE models for states 1 and 2. In this second model updating step, four parameters are optimized that were not included in the previous models. i.e. density of the fill, modulus of elasticity of the bonded fill, modulus of elasticity of the footfall sound insulation and thickness of the screed. The optimized parameter values are listed in Table 3. As can be seen, the density of the fill ρ_{bf} is about 9% smaller than the estimated initial value listed in Table 3. The largest change occurs in the elastic modulus of the bonded fill E_{bf}, which is 482 MPa after optimization (initial value = 2200 MPa). This is reasonable, as the initial value was subject to the greatest uncertainty. The modulus of elasticity of the footfall sound insulation E_f increases slightly and leads to an equivalent dynamic stiffness modulus of 13 MN/m^3. The thickness of the cement screed d_e is 1.9 cm greater than its initial value.

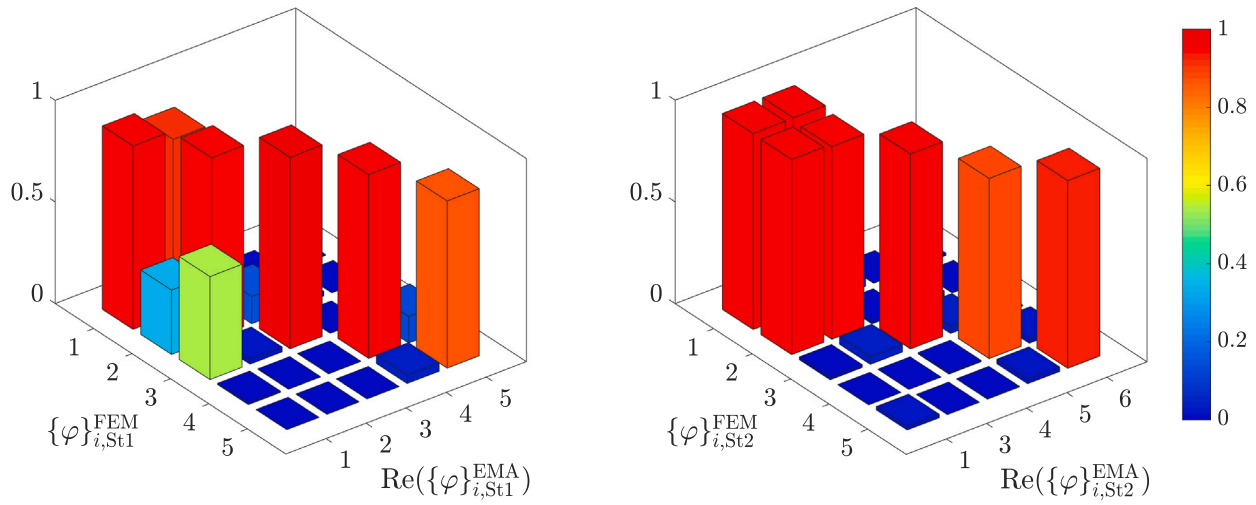

Fig. 18. Visualization of the cross-MAC matrix between the mode shapes from the FE model and the EMA in state 1 (left) and state 2 (right).

Table 2
Natural frequencies $f^{\text{FEM}}_{i,\text{St}j}$ of the FE models, MAC values $\text{MAC}_{i,\text{St}j}$, and relative errors between the natural frequencies of the FE model and the EMA $\epsilon^{(i)}_{EF,\text{St}j}$ in three construction states (construction states denoted with subscript $j = 1, 2, 3$; modal parameters denoted with subscript $i = 1, \ldots, 5$.

Mode (i)	$f^{\text{FEM}}_{i,\text{St1}}$ [Hz]	$\epsilon^{(i)}_{EF,\text{St1}}$ [%]	$\text{MAC}_{i,\text{St1}}$ [–]	$f^{\text{FEM}}_{i,\text{St2}}$ [Hz]	$\epsilon^{(i)}_{EF,\text{St2}}$ [%]	$\text{MAC}_{i,\text{St2}}$ [–]	$f^{\text{FEM}}_{i,\text{St3}}$ [Hz]	$\epsilon^{(i)}_{EF,\text{St3}}$ [%]	$\text{MAC}_{i,\text{St3}}$ [–]
1	12.50	2.18	0.90	12.02	0.00	0.96	10.81	1.25	0.96
2	14.14	1.62	0.89	15.10	2.19	0.95	13.05	–	–
3	15.89	2.67	0.94	15.86	5.04	0.96	13.73	0.05	0.90
4	24.28	3.11	0.91	22.64	2.11	0.89	15.52	1.77	0.83
5	25.95	2.89	0.82	25.45	0.02	0.92	19.76	1.99	0.94

As described above, the mass of the completed floor system has increased drastically in state 3. Since the bending stiffness of one panel joint was already identified at the upper limit at state 2, the two bending stiffnesses in the FE model of state 3 are not part of the updating process, but are set to the fixed maximum value $\gamma_{j,\text{St3}} = 1.50$ MNm/(rad m) ($j = 1, 2$).

The numerically obtained natural frequencies, MAC values and relative errors for state 3 are listed in Table 2. The mean relative error for the natural frequencies is 1.27%. Since the shaker model of the previous models is also used in the third model, there is an additional mode in the numerical model due to the shaker–structure interaction at a natural frequency of 13.05 Hz. Considering a relatively large model order in the stabilization diagram of the modal parameter estimation in Fig. 11, the stable poles at this frequency suggest that this mode is also present in the experimental data of state 3. However, since this mode has a rather low MPC value, it was excluded from the model update. The cross-MAC matrix visualized in Fig. 19 corresponds to the MAC values between the numerically and experimentally identified modes and shows the large agreement between the two sets of modal vectors. The comparison of the modes shown in Fig. 17 with those obtained from the numerical analysis (which are not shown due to lack of space) also demonstrates this good agreement.

5.4. Numerically identified modes

With the numerical model optimally adjusted to the experimental modal data, further parametric investigations can be carried out on the basis of FE analyses. Since the shaker was identified as a disturbance factor, the spring–mass system representing the shaker must first be removed from the FE models. The modal parameters computed from the FE models without the shaker then correspond to those of the floor system under consideration in the three construction states. The resulting natural frequencies are given in Table 4. The values in this table show that by installing the drywall ceiling in state 2, the fundamental frequency increases from 13.86 Hz to 15.11 Hz, although in this state the mass of the partition also contributes. However, considering that the wood battens and the gypsum fiber boards are arranged along the weaker slab direction, the drywall ceiling mainly affects the rotational stiffness of the plate joints, in addition to the increased static height of more than 20%. This leads to an increase in the natural frequency of the fundamental mode from state 1 to state 2, so that the sequence of mode shapes changes from state 1 to state 2. The change in the second frequency is negligible, while the third and fourth natural frequencies even decrease slightly. As expected, the floating screed added in state 3 leads to a decrease of all natural frequencies. This is most pronounced for the fundamental natural frequency, which decreases by approx. 4 Hz or 27% compared to state 2.

The mode shapes of the models without shaker hardly differ from those of the models with the spring–mass system, except that the modes due to the shaker–structure interaction, i.e. the fundamental modes of state 1 and 2 and the second mode of state 3 (Table 2), are missing.

Table 3
Updated parameter sets for the FE models of the three constructions states ($j = 1, 2, 3$).

Parameter	Unit	Initial	State 1	State 2	State 3
$\gamma_{1,\text{St}j}$	[MNm/(rad m)]	1.00	0.50	1.58	
$\gamma_{2,\text{St}j}$	[MNm/(rad m)]	1.00	0.29	1.13	
$k_{j,s}$	[kN/m]	215	244.6	213.2	
k_c	[MN/m]	125.7	192.0		
μ	[MN/m^2]	1.00	0.62		
s_M	[–]	1.00	1.24		
ρ_{CLT}	[kg/m^3]	490	464		
ρ_{bf}	[kg/m^3]	1600			1455
E_{bf}	[MPa]	2200			482
E_f	[MPa]	0.36			0.39
d_e	[m]	0.06			0.079

Table 4
First four numerically identified natural frequencies of the floor system without shaker $f_{i,\mathrm{St}j}$ in the three construction states ($i = 1, \ldots, 4$ and $j = 1, 2, 3$).

Mode (i)	$f_{i,\mathrm{St1}}$ [Hz]	$f_{i,\mathrm{St2}}$ [Hz]	$f_{i,\mathrm{St3}}$ [Hz]
1	13.86	15.07	10.95
2	15.81	15.86	13.46
3	24.44	22.76	15.51
4	26.04	25.51	19.80

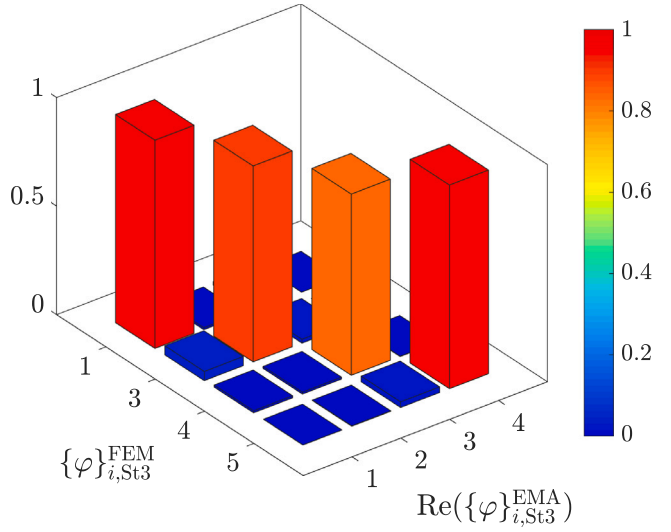

Fig. 19. Visualization of the cross-MAC matrix between the mode shapes from the FE model and the EMA in state 3.

5.4.1. Simply supported slab

To emphasize the importance of the presented model updating procedure, the results of a simple engineering model of the considered floor system are presented here. The difference to the refined model (cf. Section 3.1) of this study is that in this simple standard model the complex boundary conditions of this structure are only represented in a very simplified manner. This means that the slab is considered to be rigidly supported at the edges and at the point bearing, cf. Fig. 3. Furthermore, the elastically bound fill is only considered as an additional mass in the model. The initial values given in Section 5 are chosen as parameters for the drywall ceiling, the CLT panel, the footfall sound insulation and the screed, as they are mainly taken from currently valid codes.

The computation on this simple engineering model yield the first four natural frequencies as 8.16 Hz, 8.62 Hz, 12.62 Hz and 14.29 Hz respectively. For instance, the fundamental frequency is 25% less than that identified from the measured data in state 3. This means that with this model (as used in engineering practice) the natural frequencies of the actual system (in state 3) are massively underestimated, although the point bearing is considered rigid. This can be partly attributed to modeling the bonded fill as a mass without stiffness. Note that the bonded fill alone has twice the mass per square meter compared to the load-bearing CLT slab. The modeling inaccuracies have less effect on the mode shapes.

6. Parametric studies

With a validated FE model of the as-built floor structure now available, a wide range of numerical studies can be carried out to investigate the influence of structural changes on the dynamic behavior. As an example, a series of parametric studies related to vibrations and low-frequency sound radiation are carried out in this section.

In the first study, the influence of the material parameters of the CLT, the height of the bonded fill, the screed thickness and the spacing of the fully threaded screws in the panel joints on the natural frequencies is investigated. For the acoustic behavior of the slab system, the addition of mass in the form of fill is beneficial, but this means that load-bearing components must be sufficiently dimensioned to meet the standardized serviceability criteria for the fundamental frequency of the finished floor system.

Fig. 20(a) shows the change in the first natural frequency as a function of the material parameters, represented by the scaling factor s_M and the height of the bonded fill h_{bf}, with the numerically determined fundamental frequency of the slab highlighted by a cross-shaped marker. The values of the scale factor are chosen so that the range corresponds to the strength classes C16–C50 [26], while the height of the fill is between 0 and 15 cm. As the height of the fill decreases and thus the mass decreases, the fundamental frequency naturally increases and vice versa. As can be seen, the mass of the fill has a significant influence on the fundamental frequency compared to the material properties of the CLT. The influence of the screed thickness d_e in a range between 4 and 9 cm and the height of the fill h_{bf} on the fundamental frequency is illustrated in Fig. 20(b). The impact of the fill on the natural frequency correlates with the results in Fig. 20(a). However, a difference can be seen up to 6 cm of bonded fill, where the natural frequency decreases with increasing thickness of the screed. In these cases, therefore, the screed contributes not only additional mass but also additional stiffness.

To investigate the influence of the bending stiffness of the panel joints on the modal properties, the spacing of the fully threaded screws d_s in the panel joints is varied between 0.15 and 0.3 m. The maximum value of the rotational stiffness is estimated using the FE model described in Section 5. In Fig. 21 the normalized rotational spring stiffness $\gamma^{(n)}$ is depicted as a solid curve with cross-shaped markers. Reducing the spacing to 0.15 m results in a considerable increase in rotational stiffness of about 25% compared to the initial 0.2 m. On the other hand, increasing the distance to 0.3 m leads to a rotational stiffness to about 70% of the initial value. The natural frequencies are only computed for state 3, since the maximum rotational stiffness is fully established due to the gravity loads of the floor construction. The normalized natural frequencies $f_i^{(n)}$ are displayed with dashed lines in Fig. 21 for the first four modes. Although varying the distance of the screws has a considerable influence on the resulting rotational stiffness, the natural frequencies for the slab with floor construction change only slightly.

In the second study, the radiated sound power of the slab and the surface of the drywall ceiling is investigated in order to evaluate the influence of the parameters of the model on the vibro-acoustic performance of the slab. The steady state response of the floor system is computed using a point load with a constant amplitude of 1 N in the considered frequency range, assuming a constant modal damping ratio of 3% based on the damping ratios identified for the floor system in state 3 (Table 1). The point load is applied at the initial position of the shaker during the experimental tests. Since so far only the structural component has been investigated and thus the acoustic interaction with the receiving room has been neglected, the sound power radiated into the far field is computed with the Rayleigh integral [46] based on the velocity field of the drywall ceiling. In these investigations, the values of 8 MN/m^3, 10 MN/m^3, 12 MN/m^3 and the optimized value of 13.3 MN/m^3 are considered for the dynamic stiffness of the footfall sound insulation $s^{(i)}_{dyn}$. In Fig. 22(a) the corresponding sound power P in a frequency range between 3 and 250 Hz is shown in addition, as the focus is on the vibration behavior in the low frequency range. It can be seen that the dominant peaks of the sound power in the frequency range between about 50 and 70 Hz are shifted from the lowest dynamic stiffness value (circular markers) to the highest value (square markers). The significant increase in power at approximately 160 Hz is attributed to the drywall ceiling at the bottom of the CLT slab. However, it should be noted here that the drywall ceiling was installed on the CLT slab without acoustic decoupling in the form of sound insulation hangers.

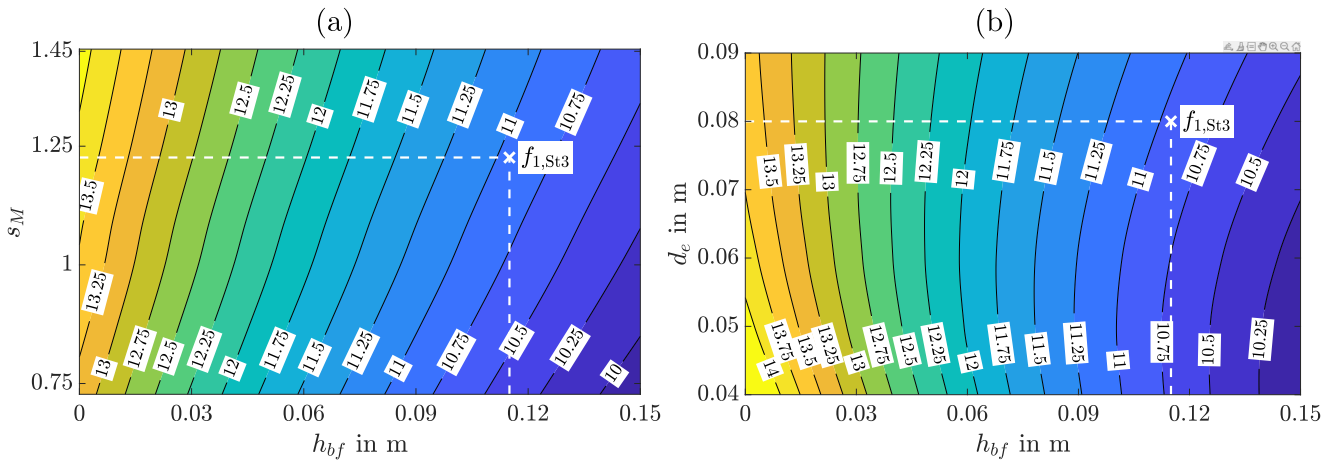

Fig. 20. Impact of (a) material parameters of the CLT represented by the scale factor s_M and (b) screed thickness over the height of the bonded fill h_{bf} on the first natural frequency $f_{1,St3}$.

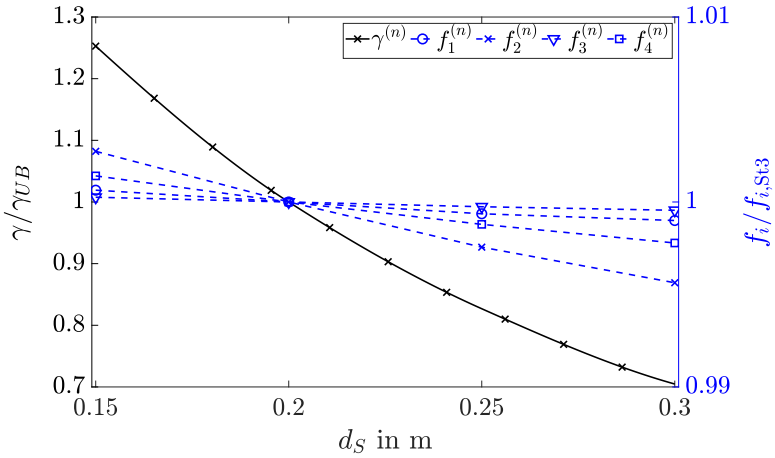

Fig. 21. Normalized rotational spring stiffness $\gamma^{(n)}$ and normalized natural frequencies $f_i^{(n)}$ $(i = 1, \ldots, 4)$ for screw distances d_s between 0.15 and 0.3 m.

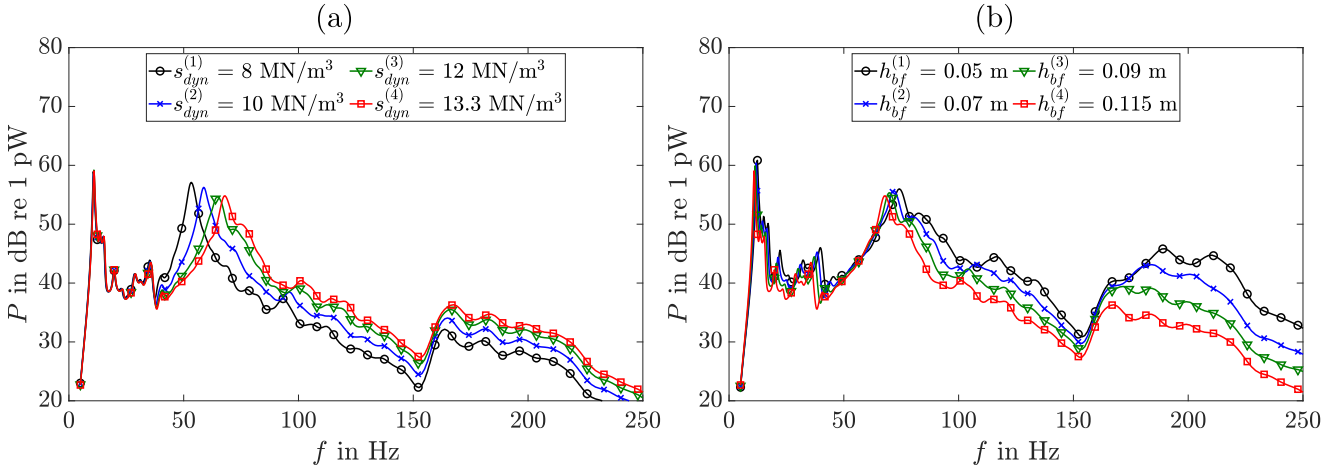

Fig. 22. Sound power P for four different values of (a) the dynamic stiffness of the footfall sound insulation $s_{dyn}^{(i)}$ and (b) the height of the bonded fill $h_{bf}^{(i)}$ $(i = 1, \ldots, 4)$.

Fig. 22(b) shows the resulting sound power for different heights of the bonded fill, i.e. $h_{bf}^{(i)}$ $(i = 1, \ldots, 4)$ = 0.05 m, 0.07 m, 0.09 m and 0.115 m. It can be seen that the reduction of the height of the fill, or rather, which is associated with a mass reduction of the floor system, increases the radiated sound power especially at frequencies larger than 100 Hz.

Fig. 23 depict the sound power for four different values of the screed thickness (i.e. $d_e^{(i)}$ = 0.05 m, 0.07 m, 0.09 m and 0.079 m) and for different values of the thickness of the gypsum fiber boards ($d_g^{(i)}$ $(i = 1, \ldots, 4)$ = 10 mm, 12.5 mm, 15 mm and 18 mm). Decreasing the screed thickness results in a frequency shift of the dominant peaks at approximately 70 Hz, also at lower total mass the amplitudes are

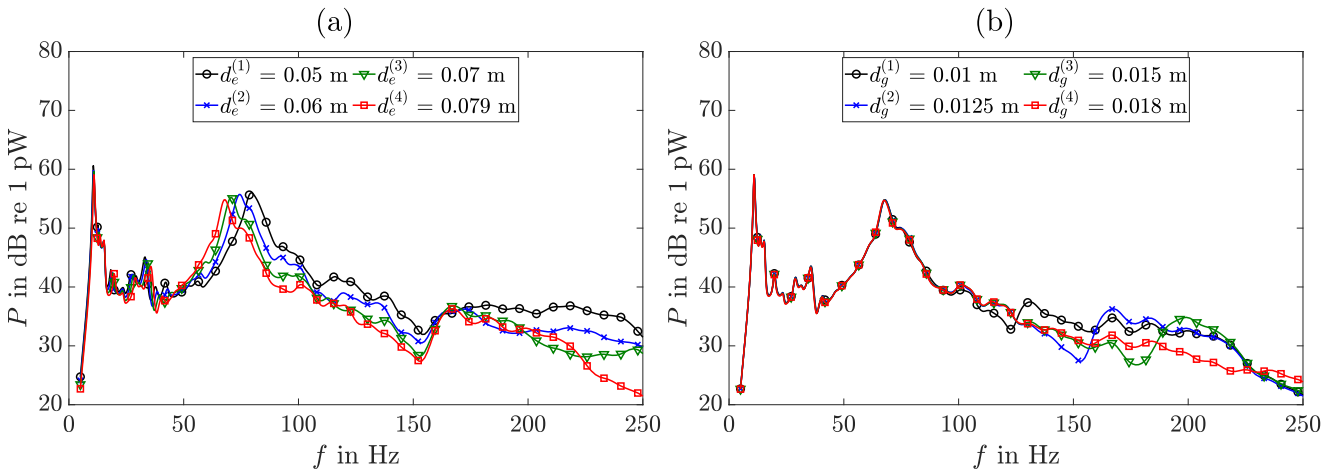

Fig. 23. Sound power P for four different values of (a) the screed thickness $d_e^{(i)}$ and (b) the thickness of the gypsum fiber boards $d_g^{(i)}$ $(i = 1, \ldots, 4)$.

slightly higher. Increasing the thickness of the gypsum fiber boards affects the sound power mainly where the modes of the fiber boards dominate. The sudden gain in power shifts with the stiffness of the boards, and it can be seen that the effect is significantly lower for the thickest boards (squared markers).

7. Discussion

With the results of this study, it could be shown that the interaction of the shaker (oscillating mass 35 kg, static mass 70 kg) with the floor structure falsifies the dynamic properties of the structure determined in EMA, especially in the first two construction states without floating screed. By omitting the shaker in the updated FE models, the influence of the shaker on the experimentally determined modal properties could be quantified. Due to this interaction, the fundamental frequency resulting from the EMA for state 1 is significantly lower by about 10% than that of the floor system (without shaker), as could be shown with computations on the FE model without shaker. Furthermore, this interaction results in similar modes that are coupled.

Another important finding is that the installation of the drywall ceiling at the bottom of the CLT slab with gypsum fiber boards leads to a substantial increase in the stiffness of the overall system, whereby between construction state 1 (without the drywall ceiling) and construction state 2 (with drywall ceiling) the fundamental frequency increases by 9%, although in the second construction state also the mass of a partition wall is present.

When the floating screed is installed, the fundamental frequency drops significantly to 10.95 Hz, which is over 27% compared to the fundamental frequency identified in state 2, as a result of the additional mass. The increase in stiffness of the entire floor system due to the screed is less significant because it is not directly fixed to the CLT slab.

Since the global behavior of the slab joints and support is nonlinear, in the refined updated FE model the equivalent linear parameters had to be found for the static deformation level under the gravity loads. Since the gravity loads are different in each state of construction, these parameters were determined separately for each of these states.

With this validated FE model, which reflects the actual dynamic properties of the considered floor system, it is possible to parametrically investigate the influence of additional nonstructural components. In the present study, the vibration behavior of the floor system in the low-frequency range was studied as an example by varying the material parameters of the CLT slab, the height of the bonded fill, the thickness of the screed and the gypsum fiber boards. The greatest influence on the fundamental frequency of the structure can be attributed to the height of the bonded fill. As the height of the fill increases, the natural frequencies decrease, on the other hand, the radiated sound power increases considerably, which must be carefully considered when designing a timber floor structure. The material parameters of the CLT slab and the screed thickness have only a minor influence on the fundamental frequency compared to the bonded fill, provided that physically reasonable values are used. Varying the spacing of the fully threaded screws in the panel joints leads to a considerable change in rotational stiffness, however, the natural frequencies of the slab with floor construction change only slightly. On the other hand, the rotational stiffness strongly affects the modal properties of the raw slab, especially the modes with one nodal line in the longitudinal direction. Finally, the impact of the dynamic stiffness of the footfall sound insulation and the thickness of the gypsum fiber boards on the radiated sound power was investigated, which contributes to the understanding of the participation of structural elements in footfall sound.

In addition, damping ratios, which are significantly influenced by the prevailing in-situ conditions, were estimated for all three construction states. Damping values of up to 8% were identified in state 1 and state 2, which can be attributed to the raw state of the floor, where gaps are present and contact between joints is not fully developed, therefore, the resulting greater friction leads to larger damping values. In contrast, the estimated damping values decreased to a maximum of 3.6% in state 3, where the gaps and joints are closed, which is attributed to the additional mass of the elastic bonded fill and screed, and consequently less energy is dissipated by friction.

8. Conclusion

In this paper, the dynamic properties of a complex timber floor system in three different construction states were investigated experimentally and numerically. From the dynamic response resulting from a frequency sweep with an electrodynamic shaker, a number of natural frequencies, modal damping parameters and natural modes of vibration of the floor structure were identified in the context of an experimental modal analysis (EMA). A finite element (FE) model was created for each of the three construction states. In a model updating procedure using the experimental results, the model parameters were determined and incorrect assumptions in the original FE models were corrected.

In the scope of this investigation, it was found that it is essential to carefully model the slab joints as well as the elastic support of the slab. It could be shown that with a relatively simple FE model as used in engineering practice, the natural frequencies of the system are significantly underestimated. This result underlines the importance of model updating, as incorrect assumptions in the initial model can be detected and corrected using the modal parameters estimated from the measured data.

In conclusion, for a timber floor system whose fundamental frequency is close to the critical lower limit, superficial modeling can lead to a distorted prediction of the dynamic and acoustic behavior. This means that if the problem is overestimated, refurbishment or design changes are carried out that are expensive but not actually necessary. On the other hand, if the problem is underestimated in the design phase, the vibration-related problems only become apparent after completion. Especially for lightweight structures with non-standard and varying boundary conditions, as they often occur in the course of reconstruction of renovation of old buildings (as in the case of the timber floor system presented in this study), the prediction of the dynamic properties with an FE model alone is a particular challenge. Information about prevailing boundary conditions, the rotational stiffness of the panel joints or the flexibility of linear and point supports is limited, highly case specific, and often state dependent. Furthermore, a number of assumptions are required to create the FE models, especially for the supports, the elastic bonded fill, and the screed, which may not fully represent the real conditions. Consequently, some input parameters must be considered as effective parameters. For instance, the thickness of the screed in the study object increased by about 30% compared to the initial value, which is due to the fact that the screed was modeled as a homogeneous isotropic layer in the FE model, although underfloor heating was also installed. Thus, for complex floor systems such as the one investigated in this study, the modeling strategy in combination with the model updating procedure can serve as a guide to reliably predicting the properties for similar lightweight wood structures.

CRediT authorship contribution statement

Michael Kawrza: Methodology, Software, Validation, Formal analysis, Visualization, Investigation, Writing – original draft. **Thomas Furtmüller:** Conceptualization, Methodology, Investigation, Writing – review & editing, Supervision. **Christoph Adam:** Conceptualization, Methodology, Resources, Writing – review & editing, Supervision.

Declaration of competing interest

The authors declare that they have no known competing financial interests or personal relationships that could have appeared to influence the work reported in this paper.

Acknowledgments

The authors would like to thank Univ.-Prof. M. Flach and S. Flach for providing the opportunity to carry out the measurements on the test object.

Appendix A. Supplementary data

Supplementary material related to this article can be found online at https://doi.org/10.1016/j.conbuildmat.2022.128032.

References

[1] R. Brandner, G. Flatscher, A. Ringhofer, G. Schickhofer, A. Thiel, Cross laminated timber (CLT): overview and development, Eur. J. Wood Wood Prod. 74 (3) (2016) 331–351.
[2] G. Schickhofer, T. Bogensperger, M. Augustin, T.U. Graz, Holz.Bau-Forschungs-GmbH (Eds.), BSPhandbuch: Holz-Massivbauweise in Brettsperrholz; Nachweise auf Basis des Neuen Europäischen Normenkonzepts [CLT Handbook: Solid Wood Construction in Cross Laminated Timber; Verifications Based on the New European Standards], second ed., Verl. TU Graz, 2010, (in German).
[3] R. Abrahamsen, Mjøstårnet - 18 storey timber building completed, in: Internationales Holzbau-Forum, 2018.
[4] P. Fast, B. Gafner, R. Jackson, J. Li, Case study: an 18 storey tall mass timber hybrid student residence at the University of British Columbia, Vancouver, in: Proc. 14th World Conference on Timber Engineering (WCTE2018), Vienna, Austria, 2016.
[5] T. Reynolds, D. Casagrande, R. Tomasi, Comparison of multi-storey cross-laminated timber and timber frame buildings by in situ modal analysis, Constr. Build. Mater. 102 (2016) 1009–1017.
[6] H. von Gierke, A. Brammer, Harris' Shock and Vibration Handbook - Effects of Shock and Vibration on Humans, McGraw-Hill, New York, 2010.
[7] L. Cremer, M. Heckl, B.A.T. Petersson, Structure-Borne Sound: Structural Vibrations and Sound Radiation at Audio Frequencies, third ed., Springer, Berlin, 2005.
[8] EN 1995-1-1: Design of Timber Structures - Part 1-1: General - Common Rules and Rules for Buildings, Standard, 2019.
[9] M. Lukacevic, J. Füssl, J. Eberhardsteiner, Discussion of common and new indicating properties for the strength grading of wooden boards, Wood Sci. Technol. 49 (3) (2015) 551–576.
[10] Forest Products Laboratory, Wood Handbook: Wood as an Engineering Material, Forest products, Madison, WI, 2010.
[11] G. Kouroussis, L. Ben Fekih, T. Descamps, Assessment of timber element mechanical properties using experimental modal analysis, Constr. Build. Mater. 134 (2017) 254–261.
[12] D. Gsell, G. Feltrin, S. Schubert, R. Steiger, M. Motavalli, Cross-laminated timber plates: Evaluation and verification of homogenized elastic properties, J. Struct. Eng. 133 (1) (2007) 132–138.
[13] P. Hamm, A. Richter, S. Winter, Floor vibrations–new results, in: Proc. 11th World Conference on Timber Engineerig (WCTE2010), Riva del Garda, Italy, 2010.
[14] H. Kreuzinger, B. Mohr, Gebrauchstauglichkeit Von Wohnungsdecken Aus Holz: Abschlußbericht, Serviceability of Wooden Floors: Final Report, Fraunhofer-IRB-Verlag, 1999, (in German).
[15] J. Weckendorf, E. Ussher, I. Smith, Dynamic response of CLT plate systems in the context of timber and hybrid construction, Composite Struct. 157 (2016) 412–423.
[16] E. Ussher, K. Arjomandi, J. Weckendorf, I. Smith, Predicting effects of design variables on modal responses of CLT floors, Structures 11 (2017) 40–48.
[17] K. Jarnerö, A. Brandt, A. Olsson, Vibration properties of a timber floor assessed in laboratory and during construction, Eng. Struct. 82 (2015) 44–54.
[18] M. Kawrza, T. Furtmüller, C. Adam, R. Maderebner, Parameter identification for a point-supported cross laminated timber slab based on experimental and numerical modal analysis, Eur. J. Wood Wood Prod. 79 (2021) 317–333.
[19] M.M. Ebadi, G. Doudak, I. Smith, Evaluation of floor vibration caused by human walking in a large glulam beam and deck floor, Eng. Struct. 196 (2019) 109349.
[20] R. Rijal, B. Samali, R. Shrestha, K. Crews, Experimental and analytical study on dynamic performance of timber floor modules (timber beams), Constr. Build. Mater. 122 (2016) 391–399.
[21] ÖNORM EN ISO 717-2: Acoustics - Rating of Sound Insulation in Buildings and of Building Elements - Part 2: Impact Sound Insulation, Standard, Austrian Standards Institute, 2021.
[22] ÖNORM EN ISO 16283-2: Acoustics - Field Measurement of Sound Insulation in Buildings and of Building Elements - Part 2: Impact Sound Insulation, Standard, Austrian Standards Institute, 2020.
[23] M. Späh, K. Hagberg, O. Bartlomé, L. Weber, P. Leistner, A. Liebl, Subjective and objective evaluation of impact noise sources in wooden buildings, Build. Acoust. 20 (3) (2013) 193–213.
[24] F. Ljunggren, C. Simmons, K. Hagberg, Correlation between sound insulation and occupants' perception – proposal of alternative single number rating of impact sound, Appl. Acoust. 85 (2014) 57–68.
[25] F. Ljunggren, C. Simmons, R. Öqvist, Correlation between sound insulation and occupants' perception – proposal of alternative single number rating of impact sound, part II, Appl. Acoust. 123 (2017) 143–151.
[26] ÖNORM EN 338: Structural Timber - Strength Classes, Standard, Austrian Standards Institute, 2016.
[27] B. Maurer, R. Maderebner, P. Zingerle, I. Färberböck, M. Flach, Point-supported flat slabs with CLT panels, in: Proc. 15th World Conference on Timber Engineering (WCTE2018), Seoul, Korea, 2018.
[28] R. Maderebner, Connecting device for mounting a wooden construction element, 2018, US20180371741 (A1), 2018-12-27.
[29] M. Billmaier, C. Bucher, A. Tributsch, Local finite element model updating with forced vibration measurements, Struct. Infrastruct. Eng. 10 (12) (2014) 1573–1594.
[30] M. Reiterer, S. Lachinger, J. Fink, S.-Z. Bruschetini-Ambro, In-situ experimental modal testing of railway bridges, Proceedings 2 (8) (2018) 413.
[31] D.J. Ewins, Modal Testing: Theory, Practice, and Application, second ed., in: Mechanical Engineering Research Studies, Research Studies Press, 2000.
[32] MATLAB, User's Guide R2019a, The MathWorks Inc., Natick, Massachusetts, 2019.
[33] P. Verboven, Frequency-Domain System Identification for Modal Analysis (Ph.D. thesis), Department of Mechanical Engineering, Vrije Universiteit Brussel, 2002.
[34] A. Brandt, Noise and Vibration Analysis: Signal Analysis and Experimental Procedures, Wiley, Chichester, 2011.
[35] W. Heylen, S. Lammens, P. Sas, Modal Analysis Theory and Testing, Katholieke Univ. Leuven Dep. Werktuigkunde, Heverlee, Belgium, 1997.

[36] R.J. Allemang, The modal assurance criterion – twenty years of use and abuse, Sound Vib. 37 (2003) 14–21.
[37] A.W. Phillips, R.J. Allemang, Normalization of experimental modal vectors to remove modal vector contamination, in: Topics in Modal Analysis II, Vol. 8, Springer International Publishing, 2014, pp. 29–41.
[38] Abaqus, ABAQUS/Standard User's Manual, Version 2016, Dassault Systèmes, 2015.
[39] J.N. Reddy, Mechanics of Laminated Composite Plates and Shells: Theory and Analysis, second ed., CRC Press, 2004.
[40] T. Furtmüller, C. Adam, An accurate higher order plate theory for vibrations of cross-laminated timber panels, Compos. Struct. 239 (2020) 112017.
[41] J.M. Whitney, Shear correction factors for orthotropic laminates under static load, J. Appl. Mech. 40 (1) (1973) 302–304.
[42] E.M. Arruda, M.C. Boyce, A three-dimensional constitutive model for the large stretch behavior of rubber elastic materials, J. Mech. Phys. Solids 41 (2) (1993) 389–412.
[43] M.I. Friswell, J.E. Mottershead, Finite Element Model Updating in Structural Dynamics, in: Solid Mechanics and its Applications, vol. 38, Kluwer Academic Publishers, 1995.
[44] P. Niemz, W.U. Sonderegger, Holzphysik: Physik des Holzes und der Holzwerkstoffe [Wood Physics: Physics of Wood and Wood-Based Materials], Fachbuchverlag Leipzig im Carl Hanser Verlag, 2017, (in German).
[45] Rothoblaas, technical data sheet xylofon, 2021, https://www.rothoblaas.com/products/soundproofing/resilient-profiles/xylofon.
[46] F. Fahy, P. Gardonio, Sound and Structural Vibration: Radiation, Transmission and Response, second ed., Elsevier Acad. Press, Amsterdam, 2007.